AN ABSTRACT OF THE THESIS OF

Mark D. Reudink for the degree of Master of Science in Electrical and Computer Engineering presented on December 19, 1991. Title: Modeling of the Orientation Dependence of Scanned HgCdTe Infrared Detectors.

Abstract approved: Redacted for Privacy

Thomas K. Plant

Mercury cadmium telluride is important in the detection of electromagnetic radiation in the eight to twelve micron atmospheric window for infrared imaging systems. High resolution infrared imaging systems use either large (256x256 element to 1024x1024 element) staring arrays or much smaller (1-6 element) scanned arrays in which the image is optically scanned across the detectors. In scanned arrays, high resolution and sensitivity may result in the scan direction not being parallel to the detector bias current.

The response of an infrared detector to uniform illumination is investigated. It is found that variations in the detector thickness result in significant changes in output voltage.

Scanned detectors are modeled in five different orientations; scan parallel to bias, scan opposite to bias, scan perpendicular to bias, and two orientations of the scan diagonal to the bias. The response is analyzed for two cases:

1) the size of the scanned radiation equal to the size of the detector and 2) when the pixel width is half of the width of the detector, but of equal length.

Results of the simulation show that the fastest response occurs when the scan and bias are parallel. The largest response occurs when the scan direction is diagonal to the bias, but the response time is much slower than when the bias is parallel to the scan. Therefore, a tradeoff must be made between maximum signal and speed of response.

Test detectors are being fabricated and will be tested at FLIR Systems Inc., Portland, Oregon, to confirm the model predictions.

Modeling of the Orientation Dependence of Scanned HgCdTe Infrared Detectors

by

Mark D. Reudink

A THESIS

submitted to

Oregon State University

in partial fulfillment of
the requirements for the
degree of

Master of Science

Completed: December 19, 1991

Commencement: June 1992

APPROVED:

Redacted for Privacy

Professor of Electrical and Computer Engineering in charge of major

Redacted for Privacy

Head of Department of Electrical and Computer Engineering

Redacted for Privacy

Dean of Graduate School

Date thesis is presented December 19, 1991

Typed by Mark Reudink

Table of Contents

List of Figures

List of Tables

Modeling of the Orientation Dependence of Scanned HgCdTe Infrared Detectors

1. Introduction

Mercury cadmium telluride (HgCdTe, HCT, or MCT) is the most widely used material for detection of radiation in the eight to twelve micron region. Its main advantage is its ability to be operated at liquid nitrogen (77 K) as opposed to liquid helium (4.2 K) temperatures.

$Hg_{1-x}Cd_xTe$ has a bandgap which varies with composition. The material can be tailored for use from one micron (x=0.8) to twelve (x=0.21) microns. Since other materials are available for detection in the three to five micron atmospheric window, $Hg_{0.79}Cd_{0.21}Te$ is relegated to the eight to twelve micron atmospheric window. The eight to twelve micron window is at the emission peak of 300 K, room temperature, black body radiation.

The primary application of $Hg_{0.79}Cd_{0.21}Te$ detectors is in infrared imaging systems used for night vision or viewing in smoke-filled rooms. HgCdTe detectors have also been used for fire detection and security systems. For example, it is possible to determine if a car has recently arrived in a parking lot due to the heat of its engine. High resolution imaging systems use large (256x256 element to 1024x1024 element) staring arrays or much smaller (1-6 element) scanned arrays in which the image is optically scanned across the

detectors.

1.1 Motivation

The response of infrared detectors in staring arrays to uniform illumination has been extensively studied. Different variations upon this theme have been investigated, such as, one, two and three dimensional effects and nonuniform illumination. Performance comparisons between scanned and staring arrays have also been studied.

For higher resolution and more sensitive imaging, more detectors must operate in unison in a scanned array. The addition of a larger number of detectors may require that the scan and bias not be in the same direction. Therefore, the effects of different scan directions on response time and signal are very important. This thesis presents results of modeling the signal output and response time of HgCdTe photodetectors to a scanned optical excitation. These results are useful in predicting optimum detector geometries for imaging systems.

1.2 Synopsis of Chapters

In the second chapter, a review of the terminology for describing infrared detectors is provided. The chapter also describes optical processes in semiconductors which are important for modeling. Finally, different methods of modeling the response of a semiconductor to radiation are

discussed.

In chapter three, the method of determining the amount of incident radiation falling upon a detector is described. The response of a detector to uniform radiation is modeled and the effects of different amounts of radiation, load resistance, and material thicknesses are studied. Next, the orientation dependence of scanned detectors is investigated and the response is modeled, for several potential orientations and two light widths.

Finally, chapter four presents a summary of the results and suggestions for additional work to extend this effort.

2. Background

This chapter introduces the terminology used for the characterization of infrared detectors, discusses optical processes in semiconductors, compares different types of infrared detectors and thermal imagers, and presents methods for modeling semiconductor detectors. Figure 2.1 displays some of the terms.

2.1 Terminology

Infrared detectors are characterized using the following parameters. Since different authors define these parameters employing different assumptions, one must determine the assumption the author uses before making comparisons.

a) Absorption Coefficient (α) is a measure of the decrease in incident radiation intensity with penetration into the material. At a given wavelength the absorption coefficient is dependent upon the density of states of the initial and final states and the probability of transition between initial and final states.

b) Bandwidth (BW) is the range of frequencies or wavelengths to which a detector can respond. The bandwidth cutoff point depends upon the author; it is usually when the signal falls to either one percent, ten percent, or three db of its maximum

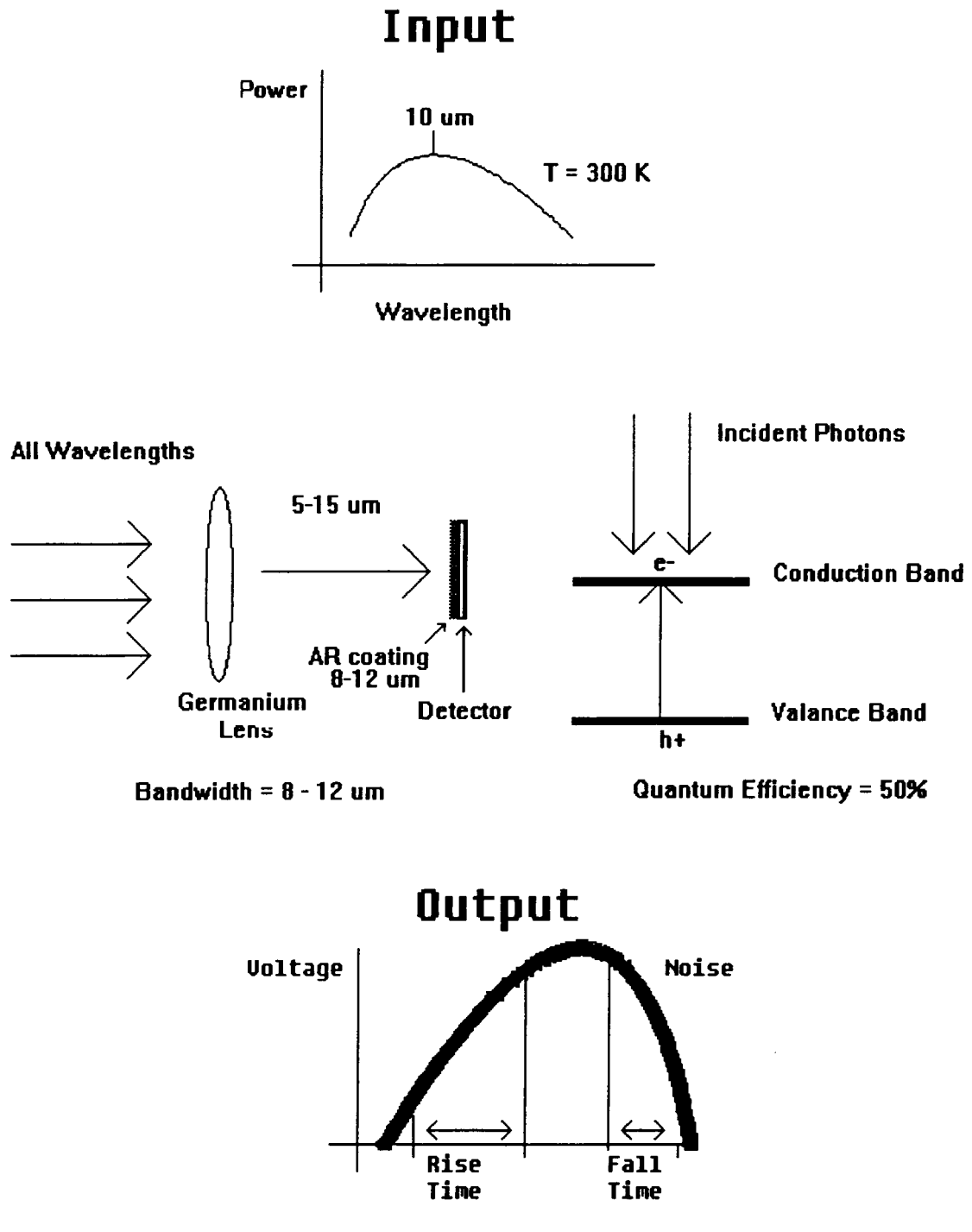

Figure 2.1 Terminology Description

value.

c) Cutoff Wavelength (λ_c) is defined as the wavelength at which the response is ten percent of the maximum response.

d) Dark Current (I_d) specifies the amount of current that flows through the detectors at a given voltage with no radiation falling on the detector.

e) Detectivity (D) and Specific Detectivity (D^*) are measures of the noise of a detection system at a certain temperature. The detectivity is defined as the reciprocal of the noise equivalent power (NEP). D^* standardizes the measure of signal to noise with respect to detector size and test conditions.

$$D^* = A^{1/2}(\Delta f)^{1/2}/NEP \quad cmHz^{1/2}/W$$

where A is the detector area and Δf is the noise bandwidth.

f) Gain (Γ) relates the number of carriers collected at the contacts of the detector to the number of electron-hole pairs generated by the incident radiation. The gain is usually a complicated function of doping levels, current density, temperature and frequency.

g) Lifetime ($\tau_{n,p}$) measures the length of time that an electron (hole) remains in the conduction (valence) band. Therefore, it is a measure of how long the electron (hole) is

contributing to the conduction process.

h) Noise Equivalent Power (NEP) stipulates the amount of incident radiation that must fall on the detector to yield a signal with magnitude equal to that of the noise.

i) Noise

There are several different mechanisms that contribute to the noise in semiconducting detector. The dominant contribution to the noise depends upon the conditions and frequency of operation.

1) 1/f Noise is associated with potential barrier effects at the contacts, surface state traps, and surface leakage currents in semiconductors. 1/f noise is predominant in the low frequency regime.

2) Generation-Recombination Noise is the dominant contribution to the noise at intermediate frequencies. It is a result of fluctuations in the generation of free carriers, either thermally or optically excited, which in turn cause variations in the carrier concentration.

3) Johnson Noise is present in all resistive materials. It is independent of frequency and depends only on temperature. Johnson noise dominates at high frequencies.

j) Quantum Efficiency (η) relates the number of electron-hole pairs generated for each incident photon at a particular

wavelength. The quantum efficiency can never be greater than unity.

$$\eta = (hc/e\lambda)\cdot R(\lambda)$$

where h is Planck's constant, c is the speed of light, e is the charge of the electron, λ is the working wavelength, and $R(\lambda)$ is the responsivity.

k) Response Time (τ_{res}) describes the amount of time it takes for an output to be seen after the detector has been irradiated. The response time gives a measure of the speed of the detector which is critical for scanned applications.

l) Responsivity ($R(\lambda)$) is the ratio of the output voltage or current to the radiant input. It is an important parameter because it gives the manufacturer an idea of the output signal for a given input irradiance. Therefore one can tell what kind of amplifiers are necessary.

m) Rise [Fall] Time (τ_r [τ_f]) is the time required for the photocurrent to rise [fall] from ten [ninety] to ten [ninety] percent of its maximum value.

n) Signal to Noise Ratio (S/N) measures the clarity of a signal. It is the signal voltage divided by the rms noise voltage.

2.2 Optical Processes in Semiconductors

The most important optical processes in semiconductors are recombination and absorption. These processes affect the semiconductor's response time, signal and noise.

2.2.1 Recombination

Bulk recombination in a semiconductor can take place via three different mechanisms; radiative, Auger, and Shockley-Read-Hall recombination. Surface recombination also plays an important role in the performance of a detector.

Radiative recombination occurs when excess carriers recombine with the emission of a photon. For example, an electron from the conduction band might recombine with a hole in the valence band as shown in Figure 2.2(a).[1] This radiative recombination process could result in the emission of a photon with energy equal to that of the bandgap of the semiconductor. Radiative recombination is important in direct gap semiconductors and only becomes important in indirect gap semiconductors when high purity is attained. The rate of radiative recombination is dependent upon the concentration of electrons and holes and the temperature.

Excitons are electron-hole pairs that orbit one another. These pairs have an energy slightly less than the bandgap. Therefore, a recombination process from an exciton to the valence band produces radiation slightly less than the bandgap of the semiconductor [see Figure 2.2(b)].

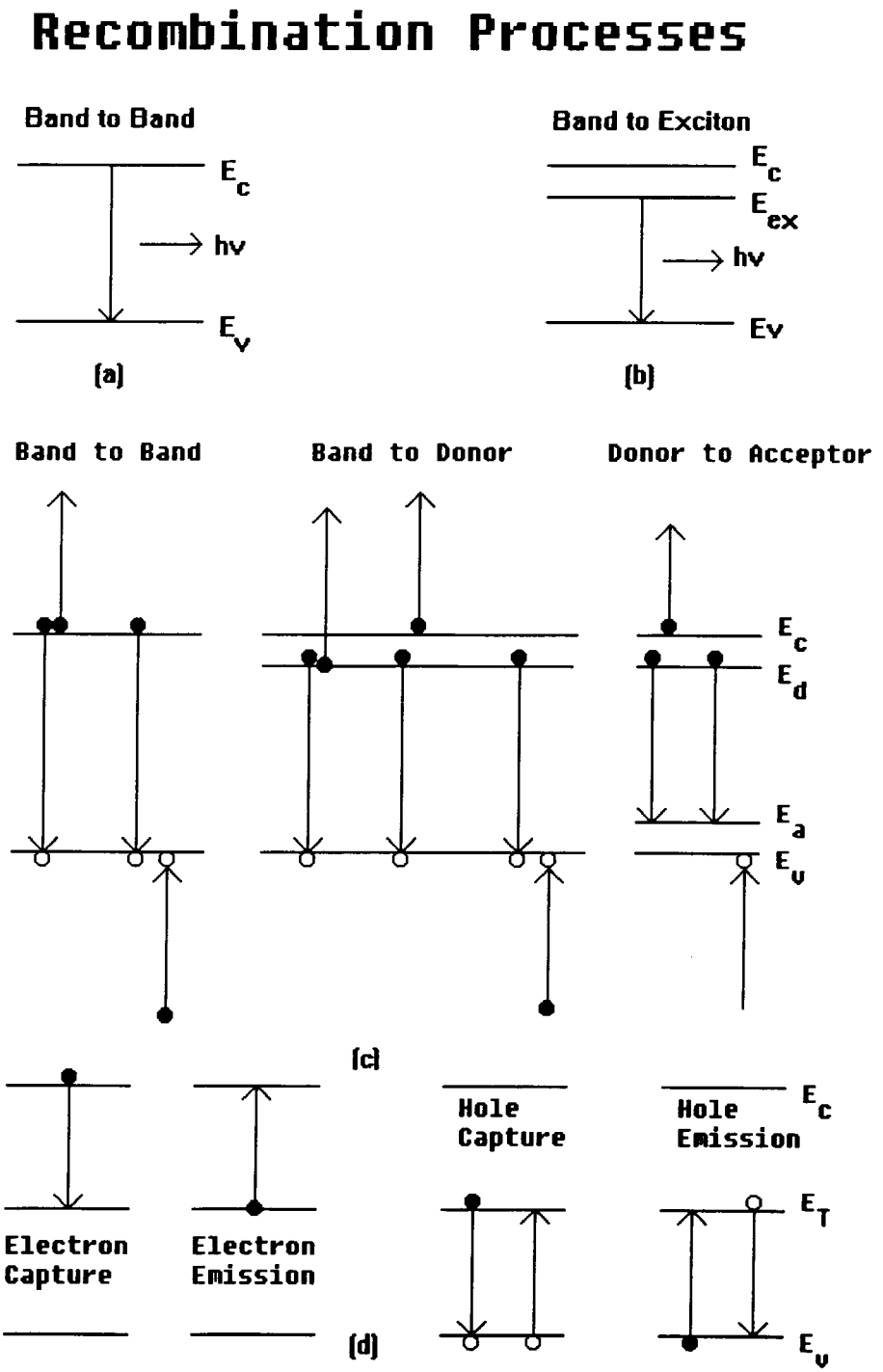

Figure 2.2 (a) Radiative Recombination; (b) Band to Excition Recombination; (c) Auger Recombination; (d) Schockley-Reed-Hall Recombination

Auger recombination is a significant recombination mechanism for heavily doped semiconductors. In Auger recombination, the energy dissipated by an excited carrier when it recombines is given to another carrier. This second carrier reduces its energy through the emission of phonons. There are several types of Auger recombination such as band-to-band, band-to-impurity, and impurity-to-impurity transitions which depend upon the doping profile. Several of the transitions are illustrated in Figure 2.2(c).[2]

In a band to band process, an electron and a hole recombine giving the energy to another conduction band electron which is excited higher into the conduction band. This electron dissipates its energy through the emission of phonons which is a radiationless process. In band-to-impurity recombination several mechanisms are possible. For example, in a donor doped material, the recombination energy can be transferred to another electron in the donor state or by an electron in the conduction band in n-type material. In p-type material the energy may be transferred to a hole in the valence band.

Recombination through trap states in the bandgap is referred to as Shockley-Read-Hall (SRH) recombination. SRH recombination is important in direct bandgap semiconductors and in semiconductors with a high concentration of deep traps. SRH recombination is the dominant recombination mechanism in HgCdTe at 77 K.[3] There are four processes associated with SRH

recombination; an electron is captured by a trap, an electron is emitted by a trap, a hole is captured by a trap, and a hole is emitted by a trap. The rate of SRH recombination is dependent upon the number of filled traps, the capture cross section, the thermal velocity, the energy of the trap and the concentration of electrons and holes.

An impurity is referred to as a trap if the probability of hole or electron capture is greater than that of emission. Traps slow the response of the photodetector and cause the photocurrent to vary as some power of the incident radiation. An impurity is considered a recombination center if the probability of electron or hole emission is greater than that of electron or hole capture. Figure 2.2(d).[4]

Since a surface perturbs the lattice, many dangling bonds may be created. These dangling bonds can create a large number of deep or shallow levels which act as recombination centers. For ohmic contacts it is desirable to have a large number of surface states, whereas for rectifying contacts a low concentration of surface states is needed.

2.2.2 Absorption

Since photodetectors operate by absorbing light, one must understand the ways in which a semiconductor can absorb photons. High energy photons, those with energies greater than the forbidden gap of the semiconductor, are absorbed by exciting an electron from the valence band into the conduction

band. Photons with energy slightly below the bandgap are absorbed through the formation of excitons or by electron transitions between the band edge and impurity states. Low energy photons are absorbed by transitions between donor states and their associated bands.

A direct bandgap semiconductor can absorb a photon ($h\nu > E_g$) directly with the excitation of an electron from the valence band to the conduction band [Figure 2.3(a)]. A free exciton occurs when $h\nu = E_g - E_x$, where $h\nu$ is the energy of the photon, E_g is the bandgap energy, and E_x is the binding energy of the exciton.

When a photon is incident upon an indirect bandgap semiconductor, a band-to-band absorption must be phonon assisted in order to conserve momentum [Figure 2.3(b)].[2] If the energy of the photon is greater than the bandgap, a phonon must be emitted to conserve momentum. If the energy of the incident photon is less than the bandgap, the excited electron must absorb a phonon in order to conserve momentum.

There are four types of band-to-impurity absorption processes. Low energy photons can be absorbed by exciting an electron from the valence band to an acceptor level or from a donor state to the conduction band [Figure 2.3(c)].[2] For transitions between ionized impurities and their respective bands, the incident photon energy must be at lead equal to the ionization energy of the impurity. An electron can be excited from the valence band to an ionized donor or from an

Absorption Processes

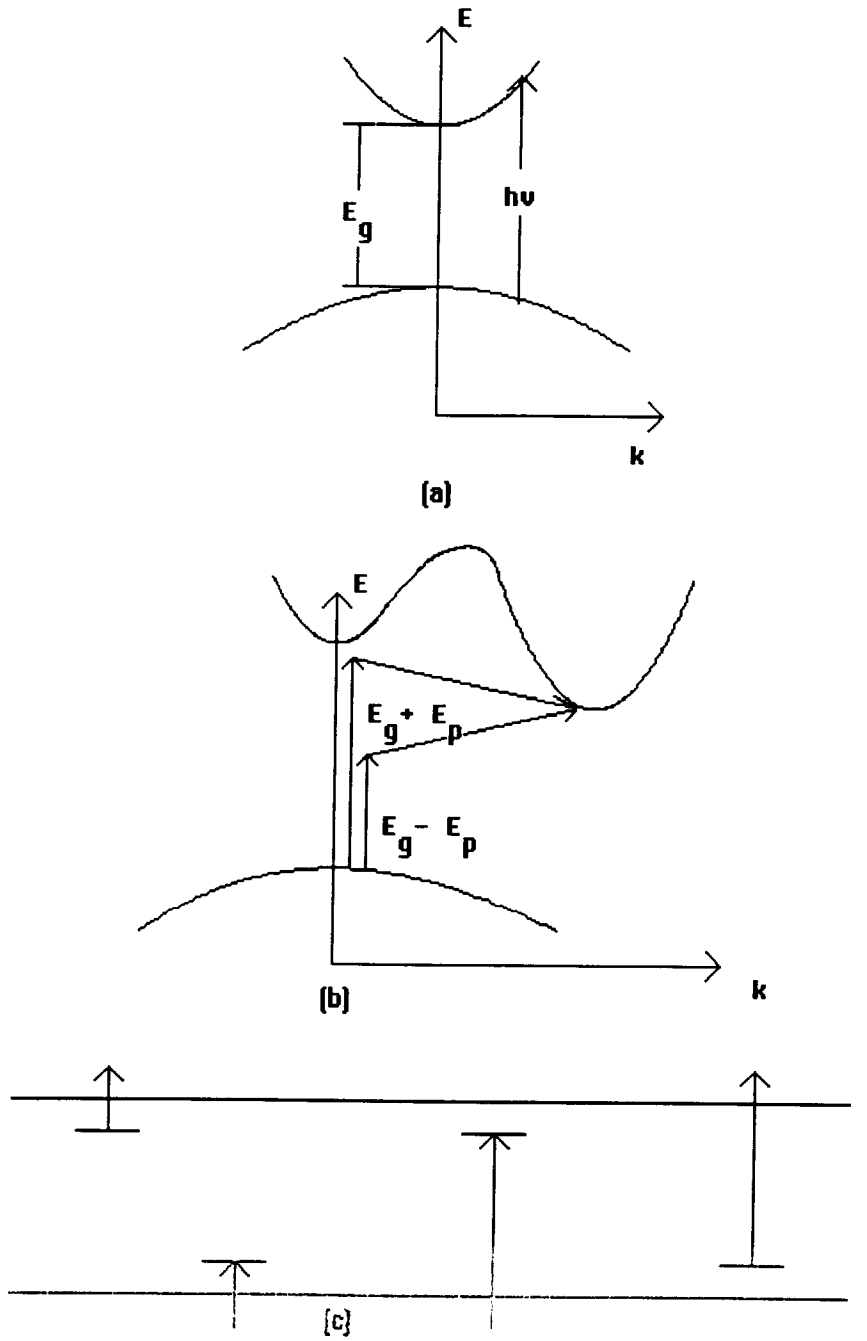

Figure 2.3 (a) Direct Bandgap Absorption; (b) Indirect Bandgap Absorption; (c) Band to Impurity Absorption

ionized acceptor to the conduction band.

2.3 Types of Semiconducting Infrared Detectors

Infrared detectors can be divided into two categories, photoconducting or photovoltaic, depending upon how they respond to infrared radiation. Photoconductive detectors are passive devices whose conductivity increases with the amount of incident radiation. Photovoltaic detectors generate a current or voltage upon absorption of radiation. The material used for a detector depends on the wavelength of the radiation, cooling capacity, and type of detector, i.e. thermal imagers, staring arrays, etc..

2.3.1 Photoconductive Detectors

Photoconductors are categorized according to the manner in which they absorb photons. Intrinsic photoconductors, lead salts and mercury cadmium telluride, absorb photons by direct transitions across the bandgap. Extrinsic photoconductors, doped silicon and germanium, absorb photons by transitions from impurity levels to their respective bands. Free carrier photoconductors, such as indium antimonide, change their conductivity through intraband transitions. In free carrier detectors, photons cause carriers to change valleys in the conduction band which changes the mobility of the carriers and, hence, the conductivity of the material.

Photoconductors are fabricated by placing ohmic contacts

on the semiconductor and passing a current through the material. Incident radiation changes the conductivity of the device which causes the current to change. The signal can be measured by recording the change in voltage across a load resistor or by monitoring the current through the device.

2.3.2 Photovoltaic Detectors

Incident radiation generates a voltage across part of the semiconductor in a photovoltaic detector. The electron-hole pairs that are generated accumulate due to local fields. These fields are a result of doping, heterojunctions, or discontinuities, such as surfaces. This accumulation of carriers generates a local space charge which is a nonequilibrium condition resulting in a potential. There are four types of photovoltaic detectors; homojunctions (Si, Ge, InSb, HgCdTe, PbSbTe), heterojunctions (PbTe/PbSbTe, GaAs/GaAlAs), Schottky Barrier (Pt/Si), and avalanche (Si, Ge-near breakdown bias).

When a photon creates an electron-hole pair in a junction device, the electron drifts to the n-type region and the hole to the p-type region. This causes a potential difference across the junction. Carriers that overcome this potential difference, ϕ_b - qV, become minority carriers and recombine. ϕ_b is the built-in potential of the junction and qV is the potential generated by the carrier separation. Photoexcited minority carriers which diffuse to the depletion region are

swept across resulting in an open-circuit voltage or a short-circuit current. The current-voltage characteristics of a junction device are rectifying, in contrast to a photoconductor which has a linear response.

Schottky barrier detectors operate in a manner similar to p-n junction devices. A semi-transparent metal film is deposited on the semiconductor and the detector is irradiated through the film. This procedure is employed when it is not possible to fabricate either a p-type or n-type region in a homojunction.

Avalanche detectors operate in high reverse bias so carriers can be accelerated across the depletion region. This gives the carriers enough energy to excite additional carriers through collisions with lattice atoms resulting in high gain.

2.4 Thermal Imagers

Infrared imagers convert incident radiation into electrical signals which are transformed into a visual display. Staring arrays and scanners comprise the two types of thermal imagers.

Staring arrays consist of a two dimensional mosaic in which each element in the array relates to a pixel on a display screen [Figure 2.4(a)]. A problem with staring arrays for imagers in the eight to twelve micron region is the need for detectors with extremely uniform responsivity and low noise. Platinum silicide and indium antimonide devices have

been fabricated with high uniformity, but they operate in the three to five micron band. Recent prototype HgCdTe staring arrays are fairly sensitive, but extremely non-uniform. The problem of nonuniformity can be avoided by scanning the image over a small, uniform detector element or linear array.

There are three different types of scan methods, serial, parallel or a combination of both. A parallel scan is performed by scanning the scene horizontally across a vertical line of detectors. A serial scan is implemented by scanning a single horizontal scene line across a single detector (or short horizontal array) and then moving to the next vertical line for the next scan. This method is similar to television and is called raster scanning. In a combination scan several serial scans are performed simultaneously using multiple serial detectors [Figure 2.5]. By limiting the number of detector elements, reasonable uniformity can be maintained.

FLIR's (Forward Looking Infrared) are the most common scanning infrared detectors. FLIR systems use a combination scanning method. Several rows of detectors are exposed to the image which is swept across the stationary detectors [Figure 2.4(b)]. In time delay integration, TDI, the signal of several scanned detectors operating in unison is summed, increasing the total signal while decreasing the total noise. The scene is sweep across the detectors using a high speed mirror rotating in the horizontal direction and a second mirror which toggles in the vertical direction. This enables

Staring and Scanned Arrays

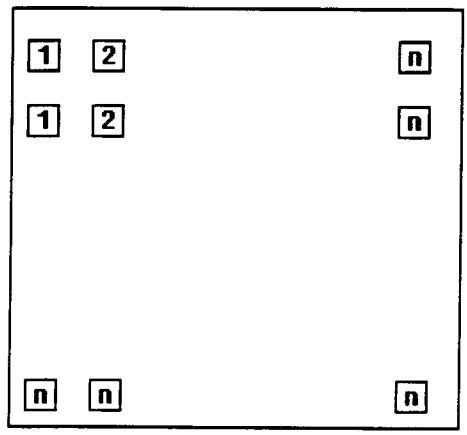

(a)

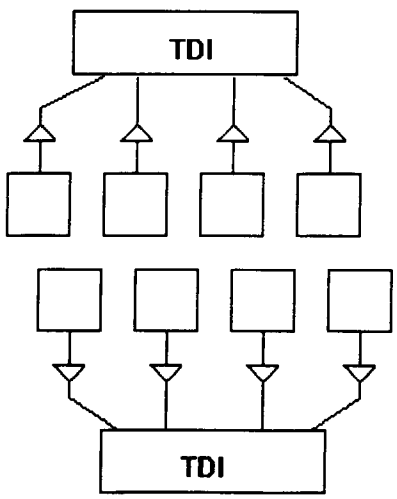

(b)

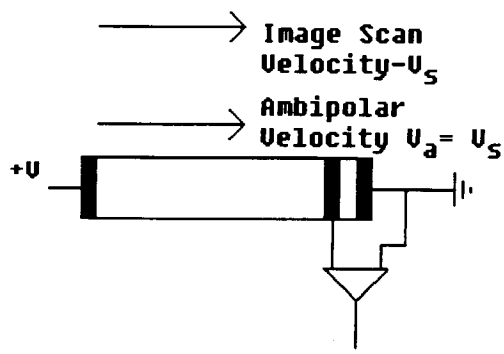

(c)

Figure 2.4 (a) Staring Array; (b) FLIR; (c) SPRITE

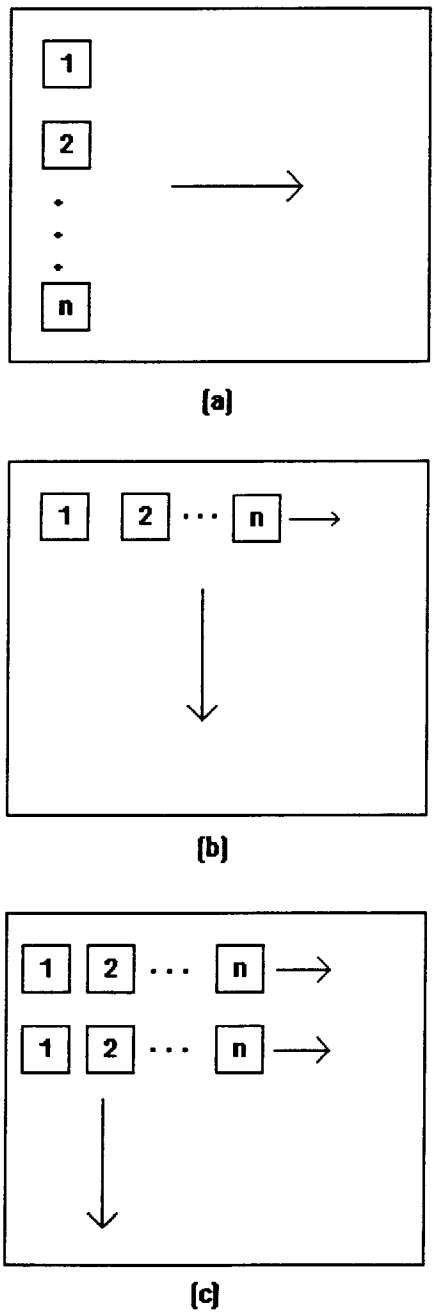

Figure 2.5 (a) Parallel Scan; (b) Series Scan; (c) SPRITE Scan

the entire scene to be scanned in a television-like manner.

SPRITE (signal processing in the element) detectors are long thin pieces of HgCdTe that have bias contacts at each end. The detector is swept across the scene at the same speed as the holes travel, resulting in an accumulation of charge. This signal is detected with a third contact which is placed near the ground bias. A SPRITE detector can achieve the same response as several individual detectors, connected in TDI.

2.5 Material Considerations

Several different materials are used to detect infrared radiation, but HgCdTe has the highest sensitivity in the eight to twelve micron atmospheric window. Although HgCdTe is very sensitive, problems of material nonuniformity persist. Figure 2.6 shows the variation in transmission and band edge wavelength present in a single HgCdTe wafer. The four curves are FTIR transmission scans through a 1mm hole at four different locations around a 15mm diameter by 0.5mm thick wafer. The wafer, obtained from Cominco, is $Hg_{1-x}Cd_xTe$ with x = 0.20 - 0.21.

Anti-reflection coating are designed to increase the sensitivity of HgCdTe photodetectors by increasing the transmission into the bulk material. ZnSe is used as an antireflection coating on HgCdTe because of a close index match and because it is not hygroscopic. Figure 2.7 demonstrates s 45% increase in transmission through a HgCdTe

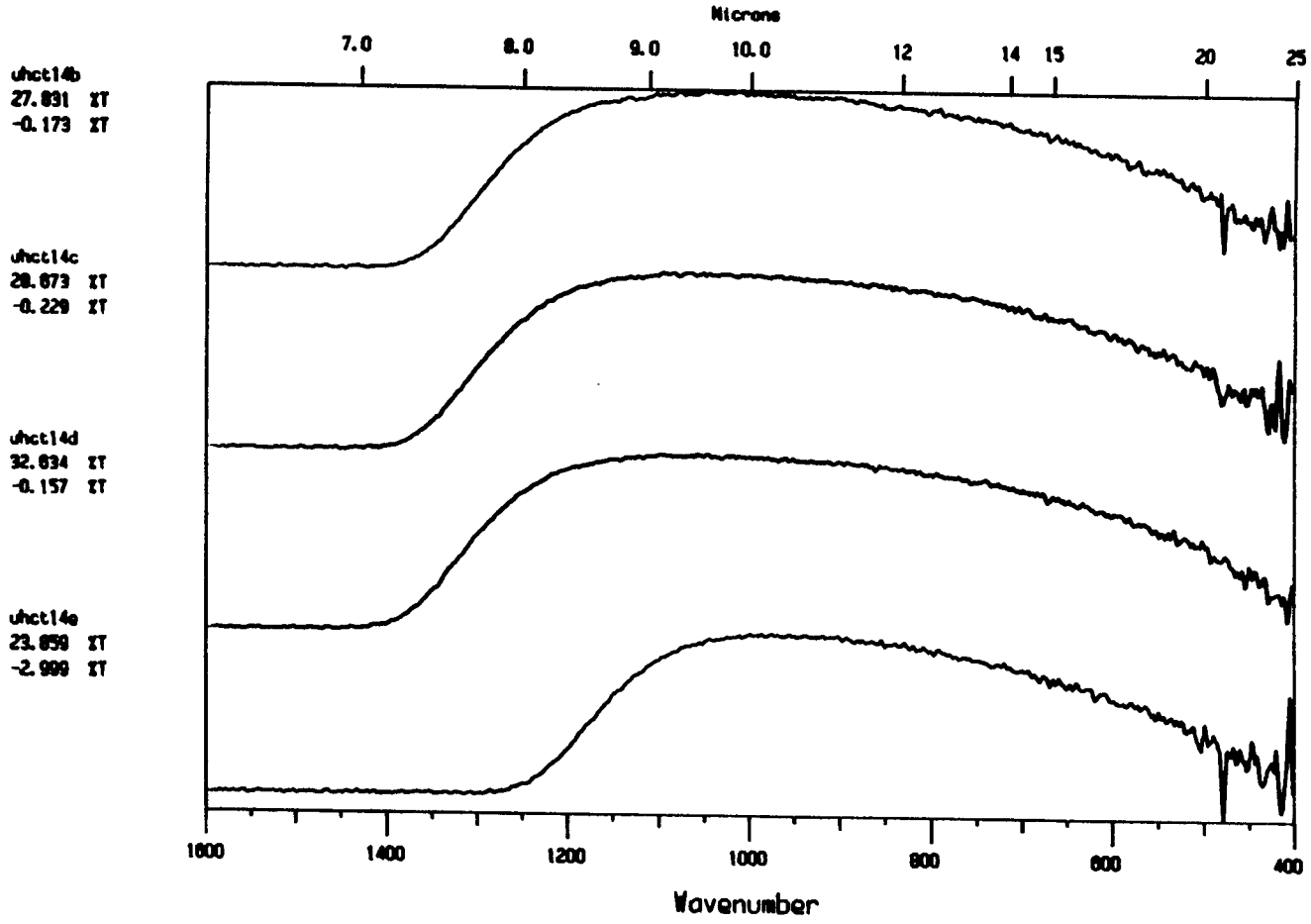

Figure 2.6 Transmission Spectra

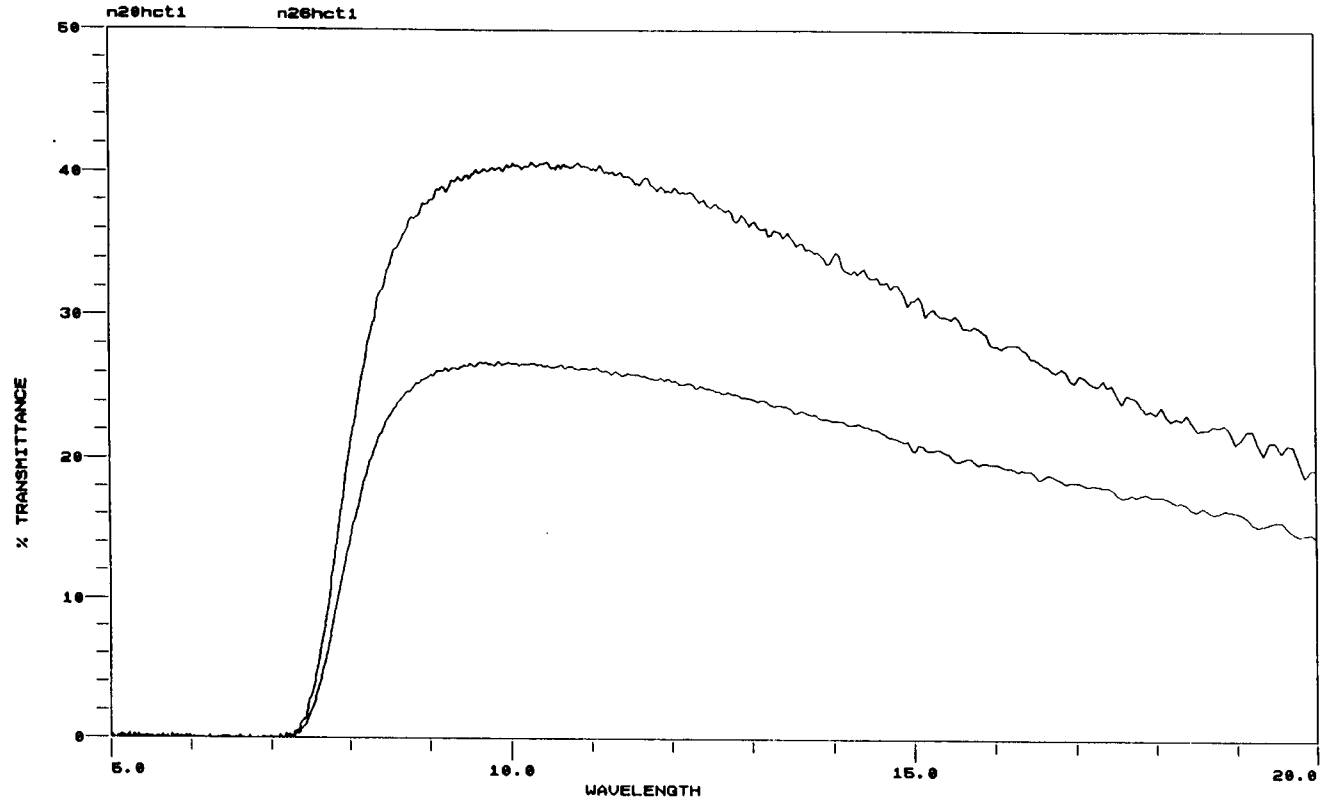

Oregon State Univ.
Chemistry Depart.
Gilbert Add'tion

Figure 2.7 Anti-Reflection Spectra

sample with the application of a ZnSe anti-reflection coating. The expected increase due alone to the anti-reflection coating is 32%. The additional transmission is probably due to passivation effects of the ZnSe on HgCdTe surface states.

The effects of different passivation layers on the performance of HgCdTe detectors is being investigated.[6] Different contact materials also alter the sensitivity of the material.[7-9]

2.6 Detector Modeling

The response of a semiconductor to photoexcitation can be modeled using several different methods. The equations that govern the diffusion of electrons and holes have been solved in one, two and three dimensions. Certain approximations must be assumed in order to analytically solve the equations. Carrier diffusion has also been modeled using Monte-Carlo random walk simulations.

2.7 Literature Review

The basic principles of infrared detector operation and testing and the supporting apparatus, including cooling systems, are described by Vincent.[10] Spiro and Schlessinger[11] provide a basis for the design of infrared systems. Photoconductive processes are characterized by Joshi.[12] Joshi also describes transient photoconductivity, noise in

photoconductors and recent developments in photoconductivity. Rose[13] describes the effects of recombination centers and traps on photoconductivity. Kingston[14] and Dennis[15] also describe the detection of infrared radiation.

Pankove[2] illustrates optical processes in semiconductors including absorption and recombination. A review of HgCdTe detector technology is provided by Rains and Broudy.[16] Several books have been written on numerical analysis and simulation of semiconductor devices.[17-19]

Modeling of photoexcited semiconductors begins with Rittner's[20] one dimensional analytical solutions to the semiconductor equations under several approximating conditions. He considers electron and hole recombination, generation, drift, diffusion and trapping.

Several two dimensional models have been analyzed. Kolodny and Kidron[21] showed that two dimensional photoconductive effects have a pronounced difference from one dimensional models in small optically-sensitive areas with planar electrodes. Shapir and Kolodny[22] investigated the response of small photovoltaic detectors to uniform radiation including the effects of surface recombination velocity and excess carrier lifetime. The effects of light attenuation on the response of longitudinal and transverse detectors was pursued by Szmulowicz, Bloch and Madarosz.[23]

The effects of lateral transport cause a significant deviation from a one dimensional model of excess carrier

distribution in semiconductor imaging arrays according to Levy and Schaman.[24] They found that the three dimensional solution differs in both magnitude and gradient from the one dimensional model resulting in a net flow of carriers much different than previously predicted. Levy, Schackman, and Kidran[25] found that a three dimensional analytical solution of the self and cross responsivity of photovoltaic detector arrays explains the reduced quantum efficiency of small detectors. An exact solution of three dimensional transport using one dimensional models was analyzed by Misiakos and Lindulm.[26] They found it was possible to use this model to find the recombination current, transit time, and open circuit voltage of planar diodes.

Transient photocurrent due to a step-function excitation in disordered materials has been studied by Arkhipov, et. all.[27] Platte[28] found that the photoconductivity in a photoexcited semiconductor transmission line depends upon the controlling light source, semiconductor material and transmission line structure.

A Monte-Carlo particle study of a semiconductor responding to a light pulse was analyzed by Moglestue.[29] Holloway[30] used a random walk treatment of carrier diffusion to relate the recombination velocity of minority carriers to the refection coefficient.

Szmulowicz, Madarasz, and Piller[31] found that the photoconductive gain of a longitudinal detector with an

arbitrary absorption profile was equal to the ratio of the average carrier lifetime to the interelectrode transit time regardless of the absorption profile of the detector. Shachman-Diamond and Kidron[32] investigated effects of internal fields on the performance of intrinsic photoconductive detectors.

Omaggio[33] analyzed the diffusion dark current in p-type HgCdTe MIS infrared detectors. The effects of surface sensitivity and bias dependence of narrow gap MSM photoconductors was examined by Darling.[34]

3. Theory

This chapter introduces the theory of the simulation of a scanned HgCdTe infrared detector. The necessary material parameters are listed along with an estimate of the incident photon flux. The simulation starts with a completely illuminated detector and progresses to scanned detectors with orientation dependence.

3.1 Material Parameters

Refer to Table 3.1 for a list of useful HgCdTe material parameters. The wafers obtained from Cominco are n-type with a donor concentration of 1×10^{14} /cm^3. Unless otherwise specified, the values listed in the table are for $Hg_{1-x}Cd_xTe$ with $x = 0.2$ and a temperature of 77 K. Typical wafers are 1.5 cm in diameter. Their poor uniformity is indicated by a 10% variation in band edge wavelength and a 25% variation in below bandgap transmission in nine sample spots around a detector at room temperature.

3.2 Estimation of Incident Photon Flux

A relationship must be found between the incident absorbed light intensity and the volume excitation rate in order to arrive at the number of carriers that are generated. Rittner[20] considers an infinite slab of semiconductor bounded by $z = 0$ and $z = d$ with Q_i photons/cm^2 s arriving at the $z =$

Table 3.1

Material Properties of $Hg_{1-x}Cd_xTe$

Dielectric Constant:

$\epsilon(0) = 17.8$ for $x = 0.2$ [35]
$\epsilon(\infty) = 13.0$ for $x = 0.2$ [35]

Index of Refraction:

$n = 3.55$ at $x = 0.21$ and $\lambda = 10\ \mu m$ and $T = 300$ K [36]
$n = 3.46$ at $x = 0.20$ and $\lambda = 10\ \mu m$ and $T = 77$ K [37]

Bandgap:

$$E_g = -0.302 + 1.93x - 0.810x^2 + 0.832x^3 + 0.535(1-2x)T/1000$$ [38]
$E_g = 0.08297$ eV at $x = 0.2$ and $T = 77$ K

Intrinsic Carrier Concentration:

$n(i) = 1.2 \times 10^{14}\ (/cm^3)$ at $x = 0.2$ and $T = 77$ K [39]

Effective Mass:

$m_e = 8.9 \times 10^{-3} m$ at $x = 0.2$ and $T = 77$ K [40]
$m_{lh} = 8.3 \times 10^{-3} m$ at $x = 0.213$ and $T = 109$ K [41]
$m_{hh} = 0.63m$ for $x = 0.205$ to 0.310 [42]

Mobility:

$\mu_e = 2 \times 10^5\ cm^2/Vs$ at $x = 0.2$ and [43]
$\mu_h = 570\ cm^2/Vs$ at $x = 0.215$ $n = 4 \times 10^{14}$ [44]
$\mu_h = 460\ cm^2/Vs$ at $x = 0.22$ and $T = 90$ K [45]

Carrier Lifetime in n-type material ($T = 77$ K):

x	$n(/cm^3)$	$t(\mu s)$	
0.20	1×10^{14}	70	[46]
0.20	1×10^{15}	1	[46]
0.20	1×10^{16}	0.01	[46]
0.23	4×10^{14}	10	[47]
0.23	1×10^{15}	1	[47]
0.23	4×10^{15}	0.1	[47]

0 surface. The relationship between the incident light intensity, I in microwatts/cm^2, and Q_i is given by

$$Q_i = \lambda I/hc$$

where h is Planck's constant and c is the speed of light.

The volume excitation rate at any plane below the surface is given by

$$f(\text{e-h pairs/cm}^3\ \text{sec}) = (1 - R)\alpha Q_i \exp(-\alpha z)$$

where R is the reflection coefficient and α is the absorption coefficient. The volume excitation rate becomes independent of z if $\alpha z \ll 1$, which indicates highly penetrating light is being used in an impurity process. For this case $f \approx (1 - R)\alpha Q_i$.

In an intrinsic process the radiation is absorbed close to the surface. If the effective diffusion length is large compared to the sample thickness, uniform volume excitation may be assumed with

$$f = (1 - R)Q_i/d.$$

At a temperature of 500 K and a wavelength band of eight to twelve microns the incident light intensity can be calculated using tables such as Czerny and Walther's Tables of the Fractional Functions of the Planck Radiation Law[48] or Pivovonsky and Nagel's Tables of Blackbody Radiation Functions.[49] Using Pivovonsky and Nagel's tables, the partial radiance $\Delta N(T)$ of an ideal blackbody source radiating at 500 K, due only to the radiation emitted in the wavelength band between eight microns and twelve microns is

$$\Delta N(T) = \{D(\lambda_1,T) - D(\lambda_2,T)\}N(T)$$

where $D(\lambda,T)$ is the relative cumulative spectral radiance of a blackbody and $N(T)$ is the total radiance of a blackbody at a given temperature. For the case at hand, $D(\lambda_1=12\mu m, T=500K) = 0.7381$, $D(\lambda_2=8\mu m, T=500K) = 0.4813$ and $N(T=500K) = 0.1129$ W cm^{-2} steradian^{-1}, therefore

$$I = \Delta N(T) = 0.029 \text{ W cm}^{-2} \text{ steradian}^{-1}.$$

The surface area of the blackbody focused onto a single detector element (a pixel) is 1 cm^2. Therefore the amount of radiation emitted by the blackbody is 0.029 W/steradian. The instantaneous field of view of the detector is 0.23 mrad by 0.23 mrad.[50] Thus, 1.53 nW of radiation fall on the detector. Since it is necessary to calculate the number of photons per cm^3, the incident power must be divided by the detector area. This yields 245 μW/cm^2 arriving at the detector.

Now that the incident light intensity has been calculated the number of photons per cm^2 incident upon the detector can be determined. This calculation yields $Q_i = 1.24 \times 10^{20}$ photons/cm^2 s.

The assumption that the volume excitation rate is independent of material thickness or the assumption that the diffusion length is long compared to the material thickness must be investigated before proceeding.

First, check if $\alpha d \ll 1$. The absorption coefficient is given by

$$\alpha = 4\pi\nu k/c = 4\pi k/\lambda$$

where k is the extinction coefficient which is given by

$$k=\sqrt{\epsilon-n^2}$$

where n is the index of refraction and ϵ is the dielectric constant. It is seen that the first assumption is not satisfied, since αd is not much less than one.

Next, one must check that the effective diffusion length is greater than the sample thickness before the assumption of a uniform volume excitation may be employed. The effective diffusion length is given by

$$L_{Diff} = [D_o \tau_o]^{1/2}$$

where

$$D_o=\frac{n_o+p_o}{n_o/D_h+p_o/D_e}$$

$$D_e=\frac{k_B T}{q}\mu_n \frac{F_{1/2}(\phi_i-E_c)}{F_{-1/2}(\phi_i-E_c)}$$

$$D_h = (k_B T/q)\mu_h,$$

and,

$$\tau_o = [B(n_o + p_o)]^{-1}.$$

Since the effective diffusion constant is dependent upon the equilibrium carrier concentrations these must first be calculated. The intrinsic Fermi level is given by

$$\phi_i=\frac{E_c-E_v}{2}+\frac{3}{4}\frac{k_B T}{q}\ln\left(\frac{m_{dh}}{m_{de}}\right)$$

where

$$m_{dh} = [m_{lh}^{3/2} + m_{hh}^{3/2}]^{2/3}$$

and

$$m_{de} = [\tfrac{1}{3}(1/m_l + 2/m_t)]^{-1}.$$

If the Fermi level is within 3kT of the band edge, Fermi-Dirac statistics must be used. If the Fermi level is not within this range, then Maxwell-Boltzman statistics may be employed. With these requirements,

$$n_o = N_c F_{1/2}[(\phi_i - E_c)/k_B t]$$

and

$$p_o = N_v \exp[(E_v - \phi_i)/k_B t]$$

where

$$N_c = 2\left(\frac{2\pi k_B T m_{de}}{h^2}\right)^{3/2}$$

$$N_v = 2\left(\frac{2\pi k_B T m_{dh}}{h^2}\right)^{3/2}$$

Before the effective lifetime, τ_o, is calculated, the recombination probability for radiative or multiphonon recombination, B, must be computed. The capture probability for direct transitions as provided by Hall[51] is

$$B_{direct} = \frac{(2\pi)^{3/2}}{3}\frac{\hbar e^2}{m^2 c^2}\eta\left(\frac{m}{m_{de}+m_{dh}}\right)^{3/2}\left(1+\frac{m}{m_{de}}+\frac{m}{m_{dh}}\right)\frac{E_g^2}{(k_B T)^{3/2}(mc^2)^{1/2}}$$

Table 3.2

Calculated Variables

I	- incident light intensity	$245\mu W/cm^2$
k	- extinction coefficient	1.14
α	- absorption coefficient(at $10\mu m$)	1.27×10^4 cm^{-1}
m_o	- electron mass	9.1×10^{-31} kg.
m_{de}	- conduction band effective mass	8.9×10^{-3} m_o
m_{dh}	- valence band effective mass	0.63 m_o
ϕ_i	- intrinsic Fermi level	0.0626 Ev
N_c	- effective conduction band density of states	2.74×10^{15} $/cm^3$
N_v	- effective valence band density of states	1.63×10^{18} $/cm^3$
n_o	- equilibrium electron concentration	1.26×10^{14} $/cm^3$
p_o	- equilibrium hole concentration	1.31×10^{14} $/cm^3$
D_e	- electron diffusion constant	1437 cm^2/s
D_h	- hole diffusion constant	3.78 cm^2/s
D_o	- effective diffusion constant	7.69 cm^2/s
B	- recombination probability	2.88×10^{-10} cm^3/s
τ_o	- effective lifetime	$13.5\mu s$
L_o	- effective diffusion length	0.01 cm
Q_i	- incident number of quanta	1.2×10^{16} photons/cm^2s
f	- volume excitation rate	8.7×10^{19} e-h pairs/cm^3s

$$B_{direct}(cm^3/s)=0.58x10^{-12}n\left(\frac{m}{m_{de}+m_{dh}}\right)^{3/2}\left(1+\frac{m}{m_{de}}+\frac{m}{m_{dh}}\right)\left(\frac{300}{T}\right)^{3/2}E_g^2$$

Since the effective diffusion length is long compared to the sample thickness a uniform volume generation can be assumed. The volume excitation rate is f = 8.7 x 10^{19} e-h pairs/cm^3 s with R = 0.3.

3.3 Uniformly Illuminated Detector

In this section, a semiconducting detector is modeled using the solution to the semiconductor equations. These equations are (1) the continuity equation for holes, (2) the continuity equation for electrons, (3) the current density for electrons, (4) the current density for holes, (5) the total current density, and (5) Poisson's equation. The generalized forms of each of these equations, respectively, are

$$\frac{\partial}{\partial t}[\delta p(r,t)]=\frac{-\delta p(r,t)}{\tau_p(t)}+G(r,t)-\frac{\nabla\cdot J_p(r,t)}{q}$$

$$\frac{\partial}{\partial t}[\delta n(r,t)]=\frac{-\delta n(r,t)}{\tau_n(t)}+G(r,t)+\frac{\nabla\cdot J_n(r,t)}{q}$$

$$J_n = q\mu_n E + qD_n \nabla n$$

$$J_p = q\mu_h E - qD_h \nabla p$$

$$J = J_n + J_p$$

$$\nabla \cdot E = \frac{\rho}{\epsilon}.$$

It is seldom possible to explicitly solve the semiconductor equations. Under certain assumptions analytical solutions can be obtained. Consider a semiconductor that is uniformly illuminated and is dominated by direct recombination. If end effects and trapping are not taken into account and low level injection is assumed, then the continuity equation reduces to

$$\frac{d\Delta p}{dt} = \frac{-\Delta p}{\tau_p} + f$$

where f is the volume excitation rate given by

$$f = (1 - R)Q_i/d,$$

and for direct recombination the lifetime is

$$\tau_p = [(n_o + p_o + \Delta p)B]^{-1}.$$

The equation to be solved that determines the fall time of a uniformly illuminated detector after the termination of illumination (f = 0) is

$$\int \frac{d\Delta p}{(n_o + p_o)\Delta p + \Delta p^2} = \int -B dt$$

The solution, subject to the boundary condition $\Delta p(t=0) = \Delta p_p$ yields

$$\Delta p = \frac{\Delta p_p e^{-B(n_o+p_o)t}}{1+[\Delta p_p/(n_o+p_o)][1-e^{-B(n_o+p_o)t}]}$$

A similar analysis gives the excess electron concentration.

A circuit can be used to model the response of the detector to the termination of steady-state illumination. A simple representation is a series combination of the detector and a load resistance with a voltage source that is used to bias the detector [Figure 3.1]. A capacitor is used to remove the DC signal from the output. The detector is modeled as a resistor with resistance

$$R = \frac{L}{\sigma A} = \frac{L}{qA(\mu_n(n_o+\Delta n)+\mu_p(p_o+\Delta p))}$$

where L is the length of the semiconductor and A is the cross sectional areas. The model uses a square detector that is 25μm on a side and 10μm thick.

A small bias voltage of less than one millivolt is applied to the circuit. The small bias is needed so that the detector is not operating is sweep out and electrons and hole recombine in the bulk semiconductor, therefore the response is due only to the recombination of the electrons and holes. When a semiconductor is operating in sweep out the holes do not recombine with the electrons until the carriers reach the contact. Since there is a large difference in the electron and hole mobility the electrons make several passes through

Equivalent Circuit

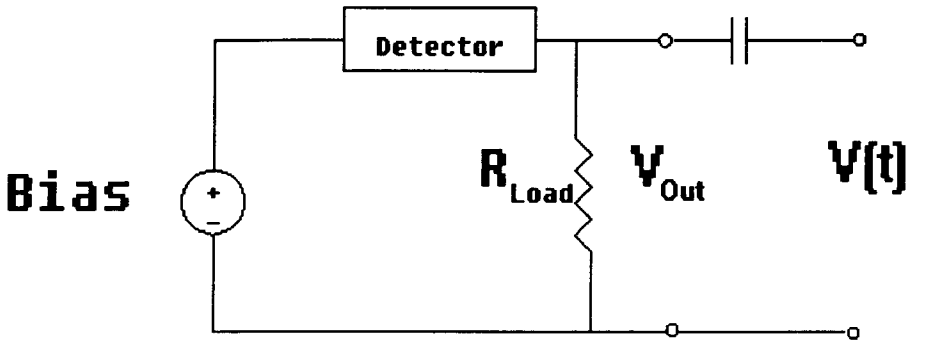

$$V_{out} = V_{Bias}\left[\frac{R_{Load}}{R_{Load} + R_{Det}}\right]$$

$$R_{Det} = \frac{L}{\sigma A}$$

$$\sigma = q[(n+\triangle n)\mu_n + (p+\triangle p)\mu_p]$$

Figure 3.1 Circuit Model

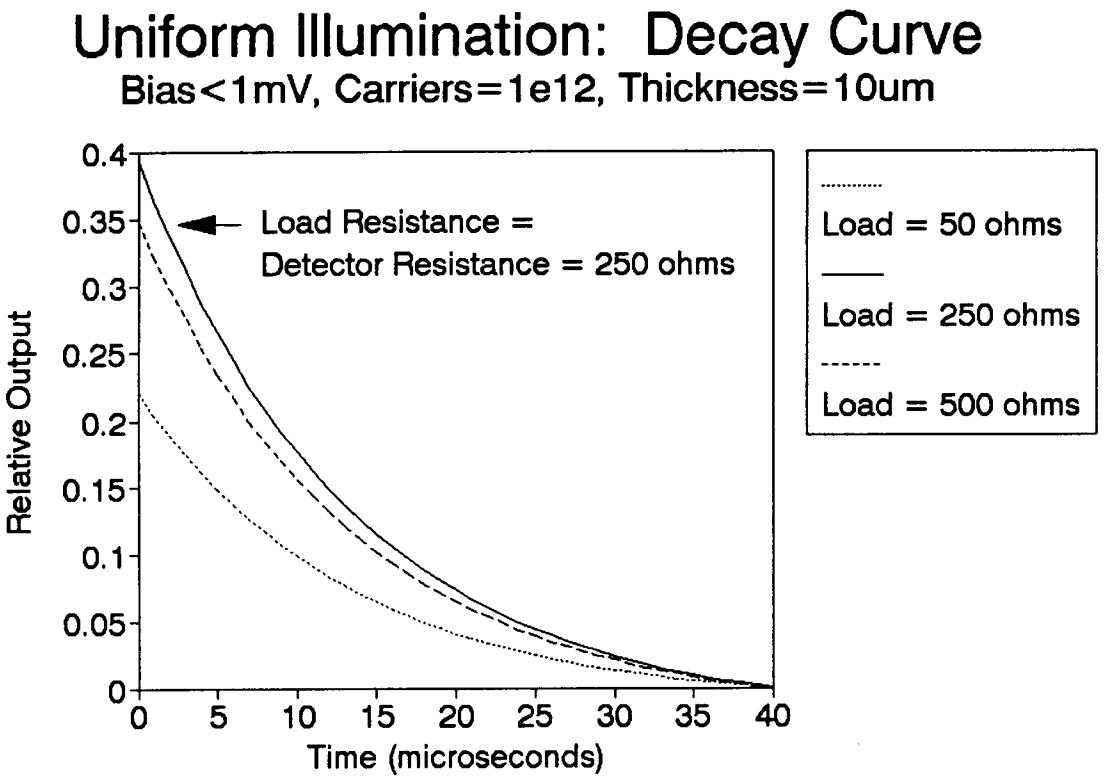

Figure 3.2 Response to termination of uniform illumination with different load resistances

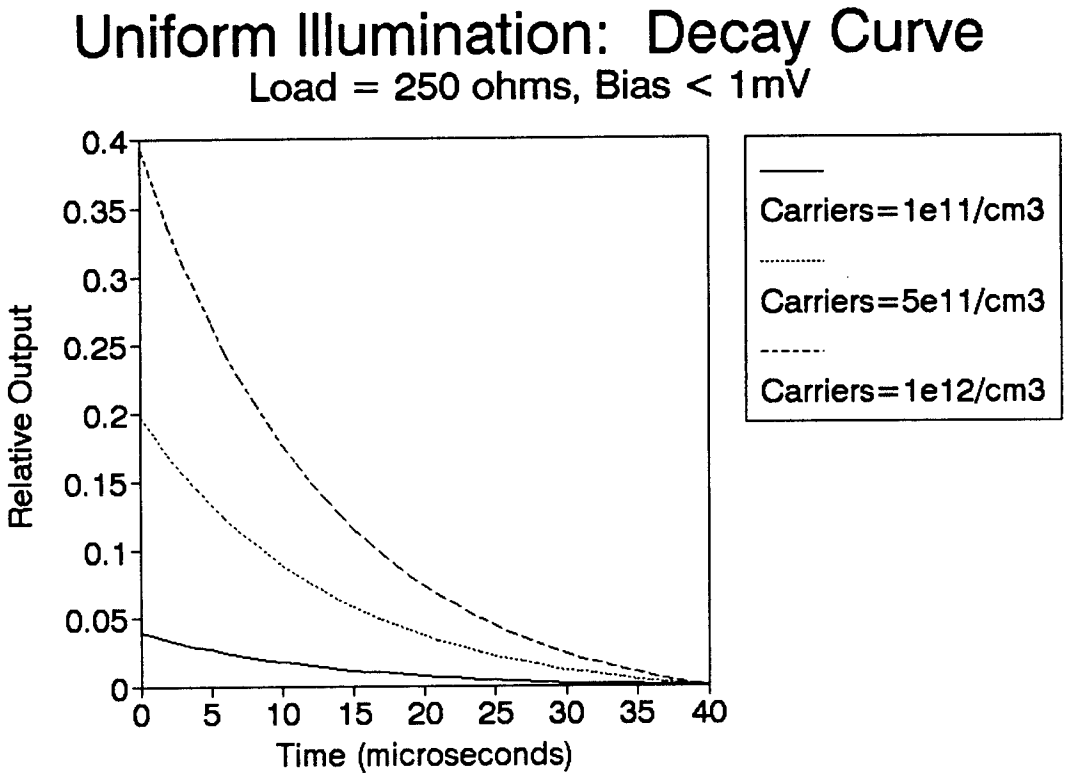

Figure 3.3 Response to termination of uniform illumination with different initial excess carrier concentrations

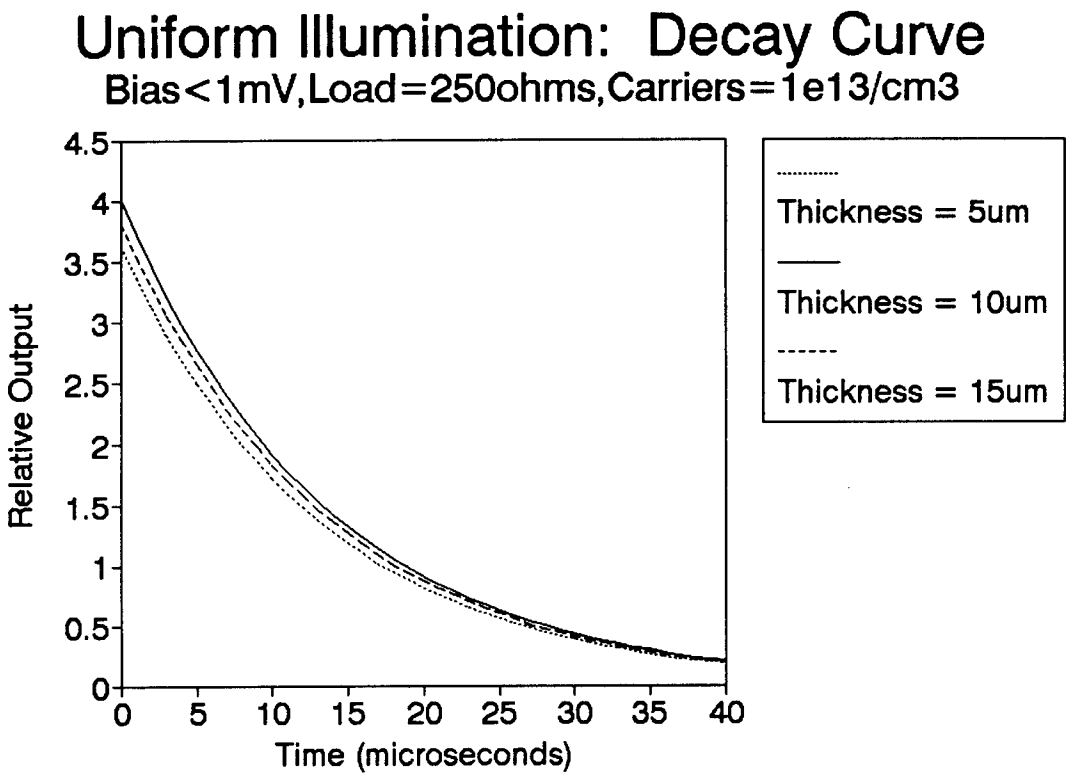

Figure 3.4 Response to termination of uniform illumination with different detector thicknesses

the semiconductor before recombining resulting in gain.

The response of the circuit to the termination of steady state illumination is plotted in Figure 3.2 for different values of excess carrier concentrations. To maintain charge neutrality the excess hole concentration must be equal to the excess electron concentration and each incident photon creates one electron-hole pair. The response is also graphed for a single excess carriers and different values of the load resistance in Figure 3.3. The output is taken across the load. The maximum change in response is detected when the load resistance is equal to the detector resistance. Figure 3.4 shows the effects of variations in thickness to the response It is seen that a small change in thickness can cause a significant difference in response.

3.4 Response of Scanned Detectors

This section analyzes the response of a HgCdTe detector scanned in five different directions with respect to the bias. The orientations are; scan direction parallel to bias, scan direction opposite bias, scan direction perpendicular to bias, and two orientations of the scan direction diagonal to bias. [Figure 3.5(a,b,c,d,e)].

3.4.1 Assumptions

In this model an eighty percent quantum efficiency is assumed. Therefore, each 100 incident photon creates 80

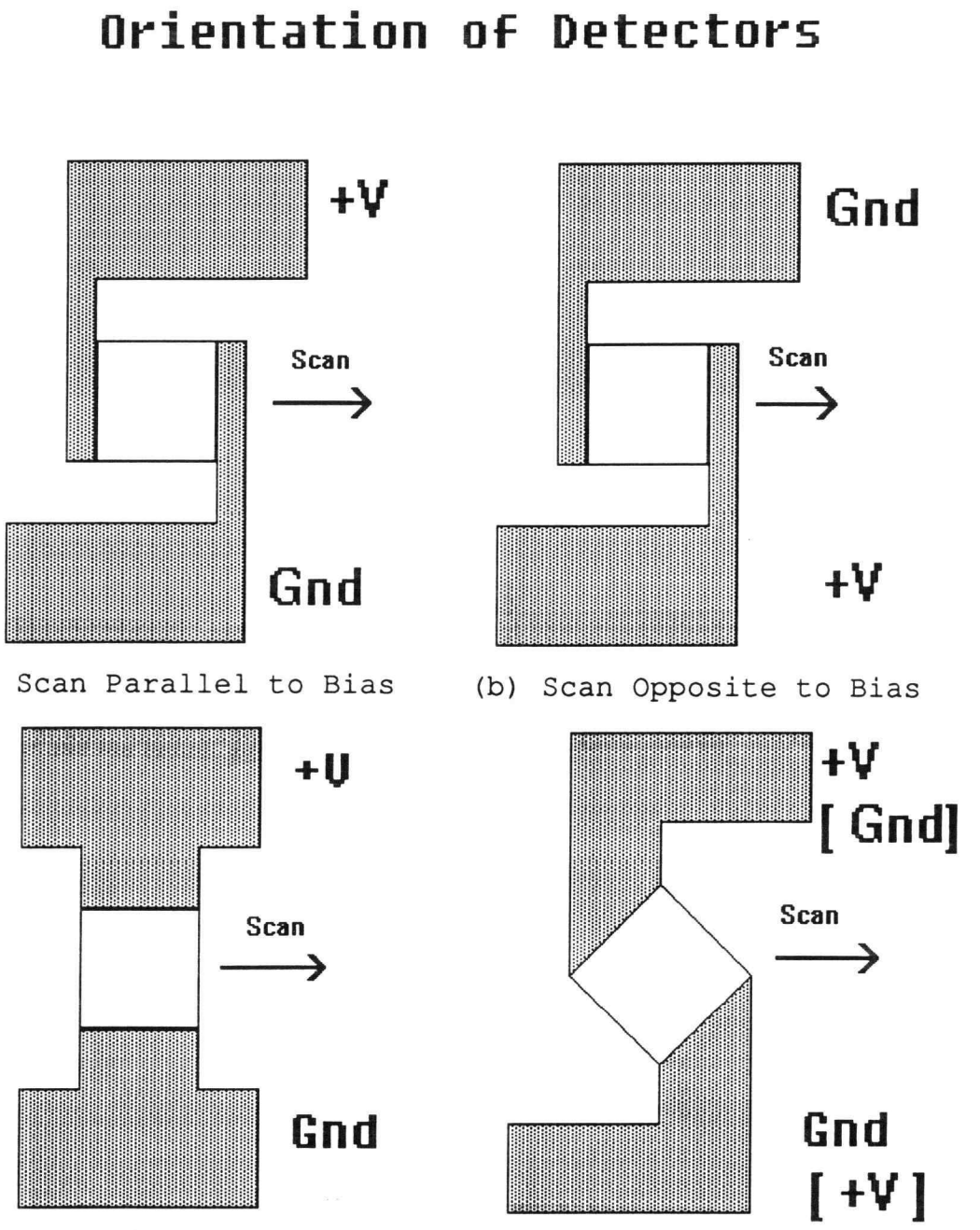

(a) Scan Parallel to Bias

(b) Scan Opposite to Bias

(c) Scan Perpendicular to Bias

(d) Scan Diagonal to Bias (+)
(e) Scan Diagonal to Bias (-)

Figure 3.5 Scan Orientations

electron-hole pairs. It is also assumed that the detector is being operated in sweep out, therefore no recombination takes place within the semiconductor and holes recombine at the contacts while the electrons can make many passes through the semiconductor resulting in

electron-hole pairs. It is also assumed that the detector is being operated in sweep out, therefore no recombination takes place within the semiconductor and holes recombine at the contacts while the electrons can make many passes through the semiconductor resulting in gain. The incident light is scanned at the hole velocity.

3.4.2 Basic Model

The motion of the electrons and holes must be investigated in order to model the response of the scanned detector. If the detector is divided into N equal parts, the number of electrons and holes can be counted in each increment. It is assumed that an equal number of electrons and holes are created in each division to maintain charge neutrality. Since the electron mobility is many times greater than the hole mobility, the electrons can make several passes through the circuit before recombining at the contact.

The detector is scanned at 3.85×10^4 cm/s. This speed is chosen so that the optical system operates at the same speed as commercially available monitors. The image enters the optical system through a germanium lens and is focused

onto a mirror rotating at 78,750 rpm. The rotating mirror directs the beam onto a second mirror which toggles in the vertical direction allowing the image to be scanned across the detectors at which point the image is detected as a change in current or voltage across a resistor.

Since the hole mobility is 460 cm^2/Vs, the applied electric field must be 84 V/cm in order for the scan speed to equal the hole velocity. This corresponds to a 210 mV bias for a 25 μm long detector. The electron velocity is therefore 1.68×10^7 cm/s. With the scan speed stated above it takes the light 132 ns to traverse the detector. Since the electron and hole lifetimes are on the order of microseconds the approximation that they will not recombine in the semiconductor is reasonable. If the detector is divided into sixty-six one nanosecond divisions, the electrons will make 6.7 passes through the semiconductor for each one nanosecond step the holes take. The electrons and holes do not recombine until the holes reach the contact. The gain is a result of the large discrepancy in the mobility of the electrons and holes.

Each of the responses are shown for the circuit model of Figure 3.1. The bias is 210 mV and the output is taken across a 400 ohm load resistor. A 400 ohm load resistor is used since it results in the optimal S/N value.

3.4.3 Scan Direction Parallel to Bias

When the detector is biased in the same direction as the scan the electrons and holes do not start to recombine until the light is completely covering the detector. This is a result of the light and the holes are travelling at the same velocity and in the same direction. The electrons and holes will continue to recombine at the contact until the light has left the detector.

The calculated response of the detector is shown in Figure 3.6 for the case in which the width of the light is the same as the width of the detector and for the case where the light width is half the width of the detector.

3.4.4 Scan Direction Opposite to Bias

When the scan direction is opposite to the bias the holes reach the contact immediately. Therefore, the electrons and holes begin to recombine as soon as the light first hits the detector. When the light is almost off the detector, holes continue to be created and must traverse the full width of the detector before recombining at the ground contact. Thus, recombination continues after the detector is no longer being illuminated.

The calculated response of the detector is shown in Figure 3.7 for the case in which the width of the light is the same as the width of the detector and for the case where the light width is half the width of the detector.

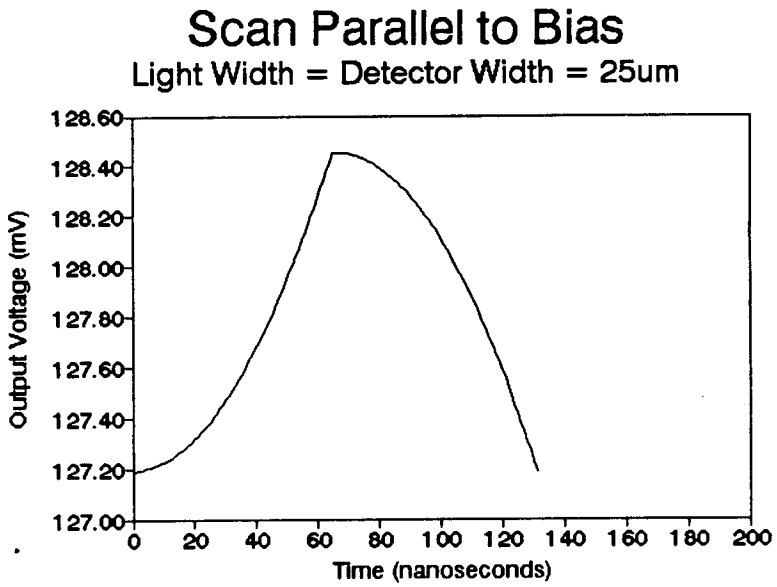

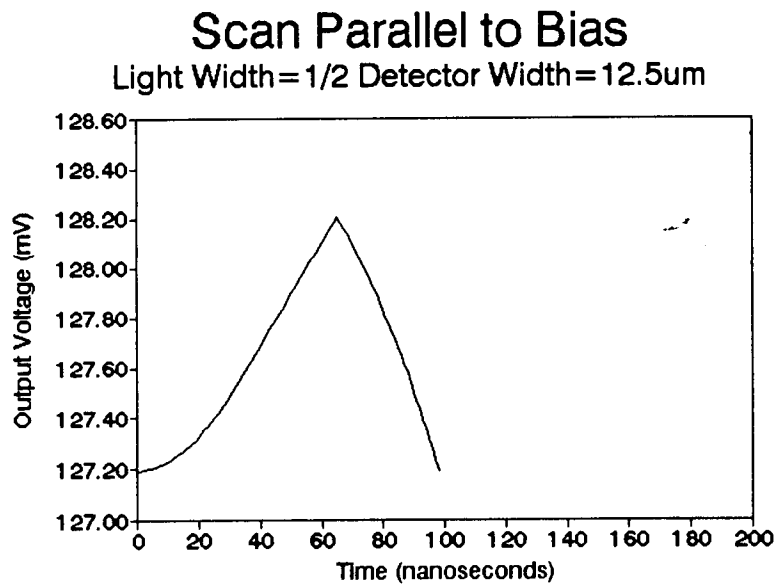

Figure 3.6 Response of Scan Parallel to Bias

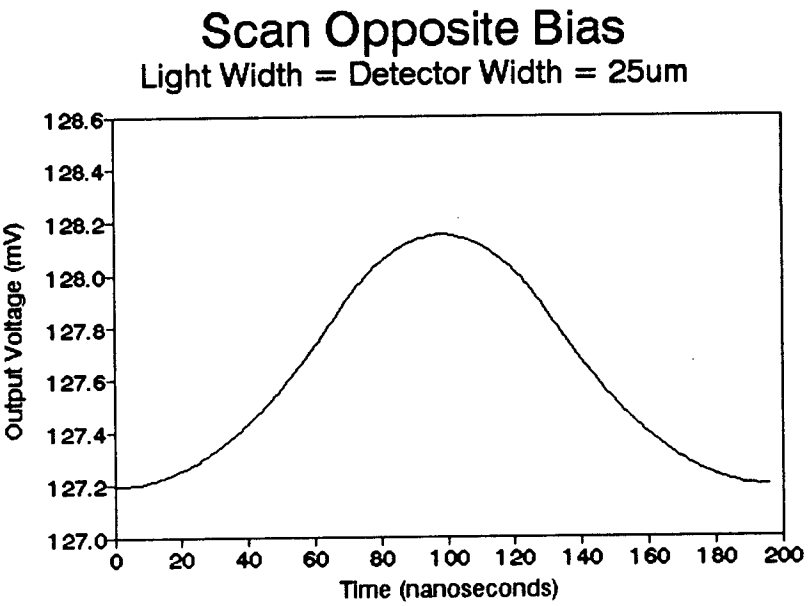

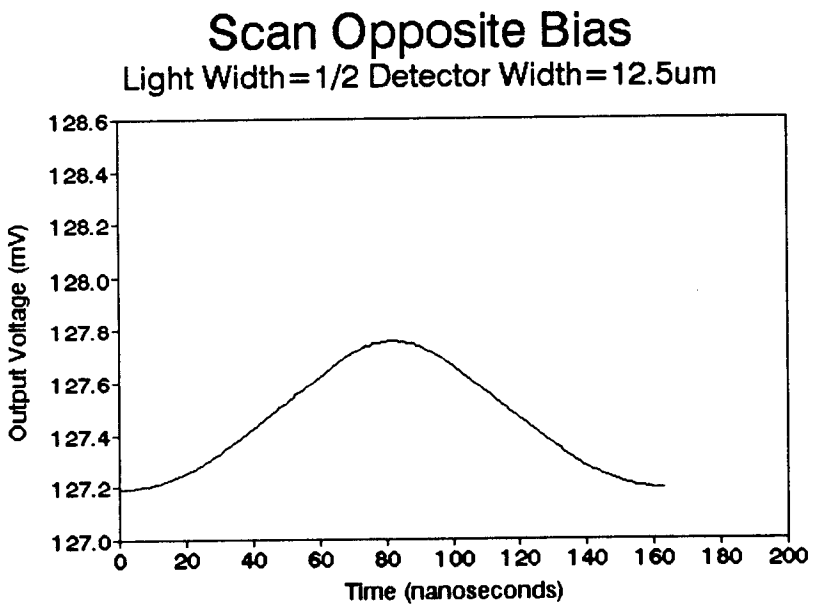

Figure 3.7 Response of Scan Opposite to Bias

3.4.5 Scan Direction Perpendicular to Bias

Electrons and holes recombine as soon as the detector is illuminated when the scan is perpendicular to the bias. Analogous to the scan opposite to the bias the electrons and holes continue to recombine after the detector is no longer illuminated. In Figure 3.8 the response is plotted for the light width equal to and half of the detector width.

3.4.6 Scan Direction Diagonal to Bias

There are two different possibilities for biasing in the diagonal orientation. When the top contacted is positively biased and the bottom contact grounded as shown in Figure 3.5(d), the electrons and holes do not recombine until the light has travelled across half of the detector. When the top contact is grounded and the bottom contact has a positive bias as shown in Figure 3.5(e), the electrons and holes begin to recombine immediately. When the scan direction is diagonal to the bias part of the detector is never illuminated.

The response is shown when the light width is the same width as the detector and when the light width is half of the width of the detector. For both cases the length of the light is the same as the length of the detector, but only $1/\sqrt{2}$ of the diagonal dimension. Figure 3.9 shows the response when the top contact is at a positive potential and the bottom contact is grounded and figure 3.10 shows the response when the top contact is grounded and the bottom contact is at a

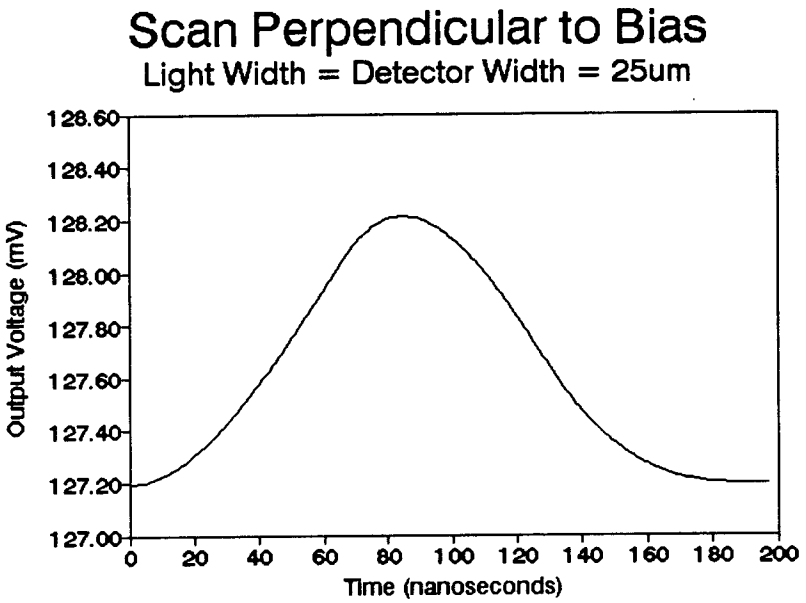

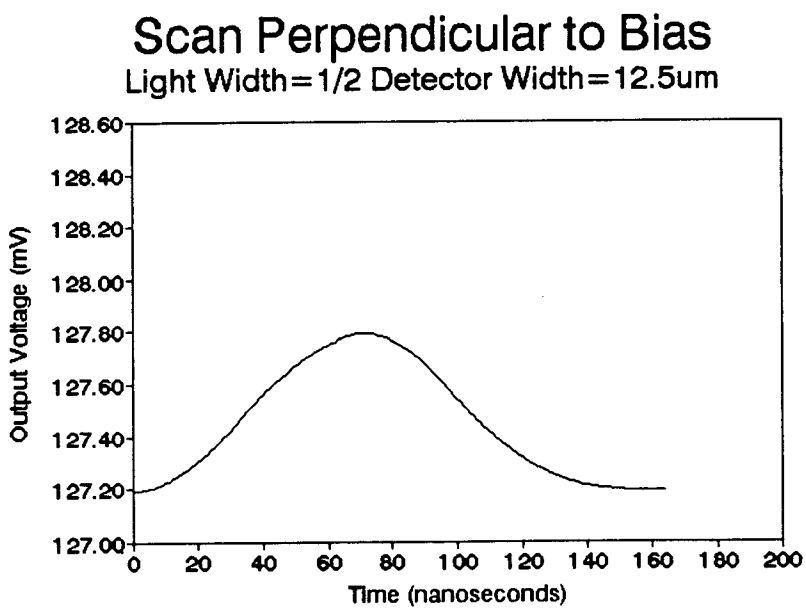

Figure 3.8 Response of Scan Perpendicular to Bias

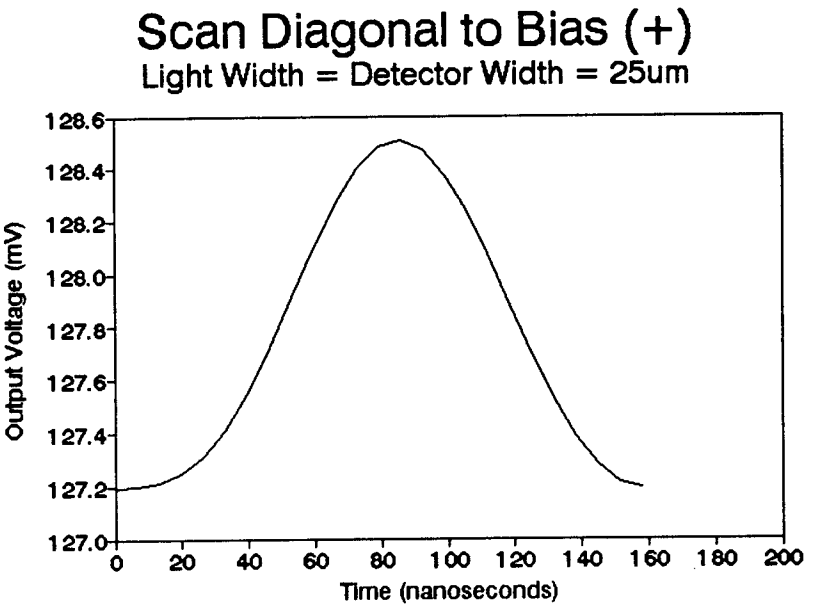

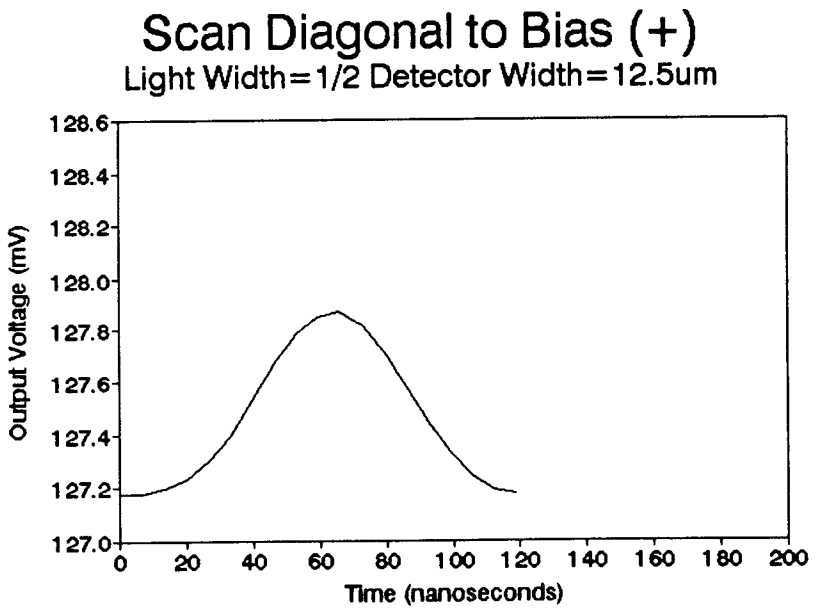

Figure 3.9 Response of Scan Diagonal to Bias (+)

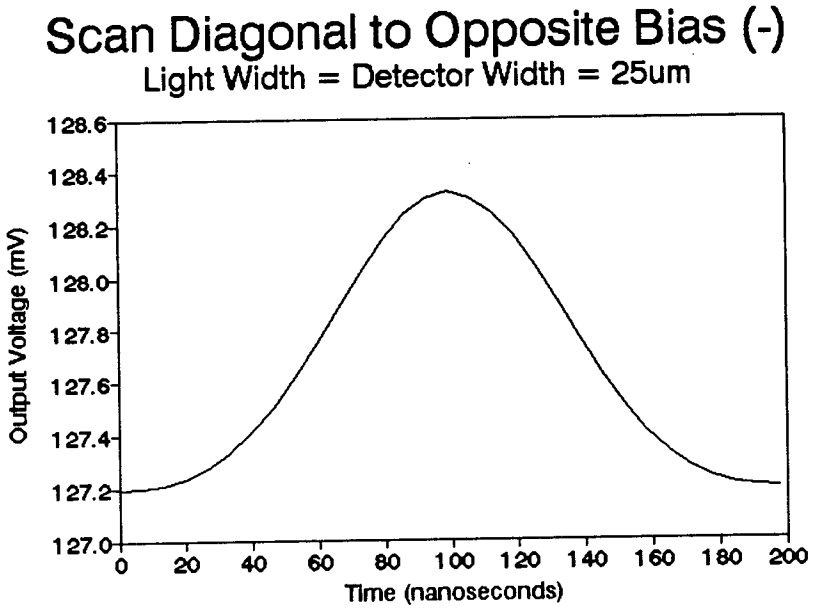

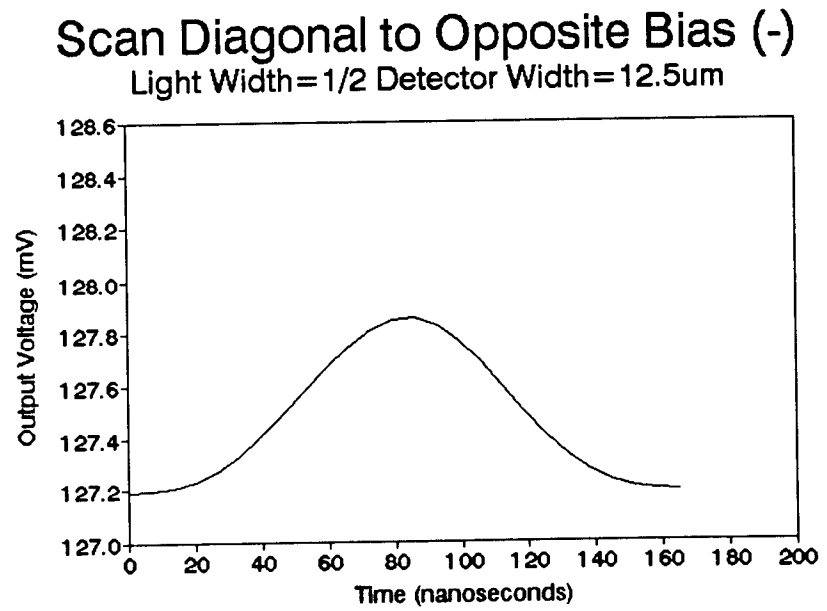

Figure 3.10 Response of Scan Diagonal to Bias (-)

positive potential.

3.5 Preliminary Experimental Data

A "four bar target" is used to measure the response of HgCdTe infrared detectors. The experimental setup consists of a flat plate heated to temperature T > 300 K behind a room temperature (300 K) flat aluminum plate with four long, narrow slots equally spaced by the narrow aluminum remaining between the slots. When the "four bar target" is projected onto the detector, the image width of the hotter slot is the same width as the detector, but the length of the slot is much longer than the detector.

The experimental data was taken at FLIR System Inc., Portland, Oregon. A square two mil (50 micron) detector was rotated through 360 degrees in order to obtain the different orientations of the scan with respect to the bias. Rotating a single detector alleviates problems of material nonuniformity which would be encountered if each detector orientation was fabricated on a separate section of HgCdTe.

Figures 3.11 and 3.12 show the response from a square two mil (50 micron) detector. When the bias is in the same direction as the scan, four separate responses are observed due to the four bars. When the detector is perpendicular to the bias or diagonal to the bias four separate responses are not observed. This results because the fall time of the detectors is not fast enough to distinguish between the four

bars. Therefore, before the response can decay from the first bar the detector begins to respond to the second bar making the bars indistinguishable.

It is also possible to observe the response time from the data. When the bias is parallel to the scan the response time is the fastest and when the bias is diagonal (-) to the scan the response is the slowest as the model predicts.

The voltage scale on the photographs is calibrated so that a reading of 100 on the photograph corresponds to a voltage of 715 mV. It is also observed from the data that the voltage response does not vary significantly from orientation to orientation. The model predicts that this will be the case for square detectors.

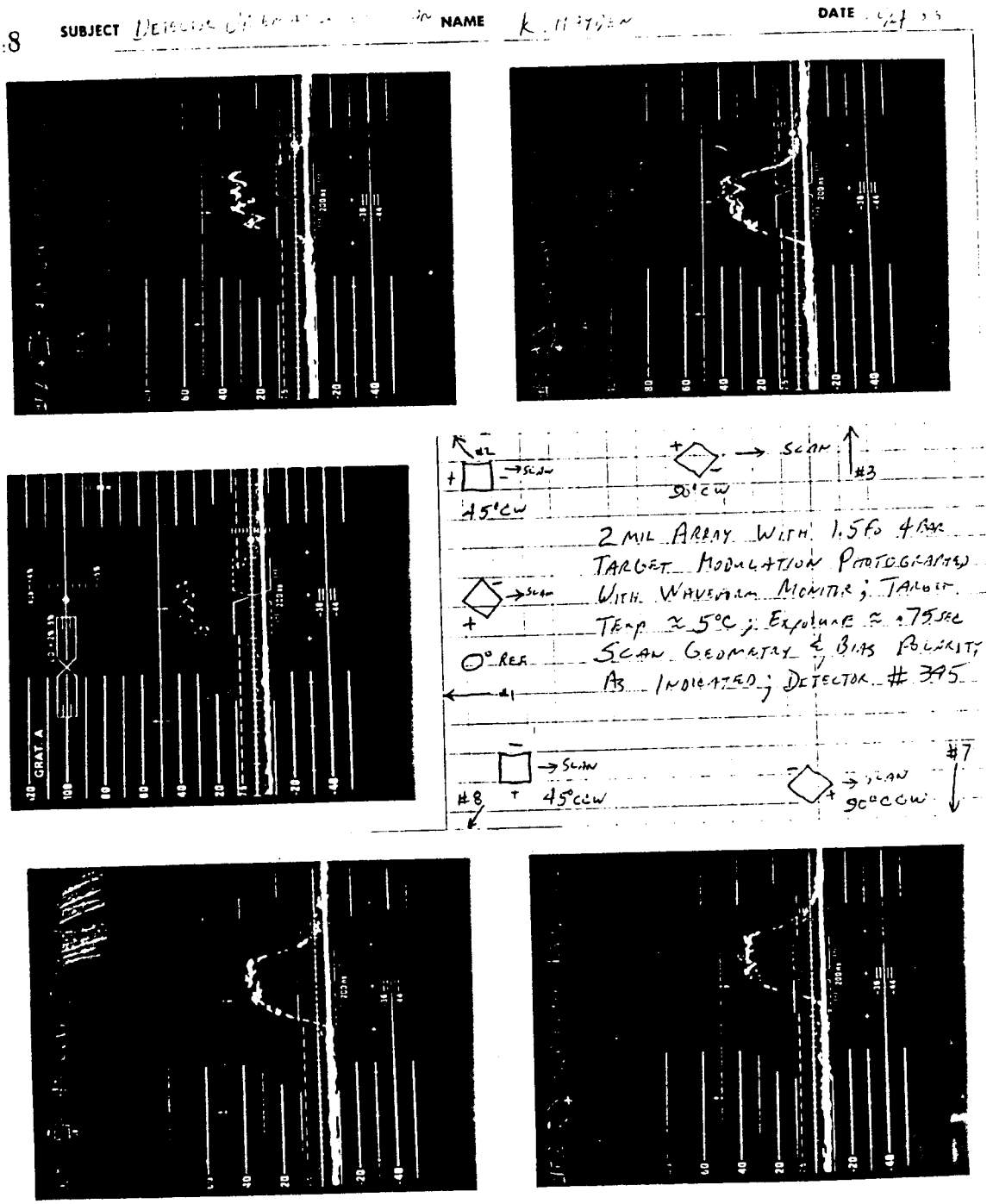

Figure 3.11 Preliminary Experimental Data

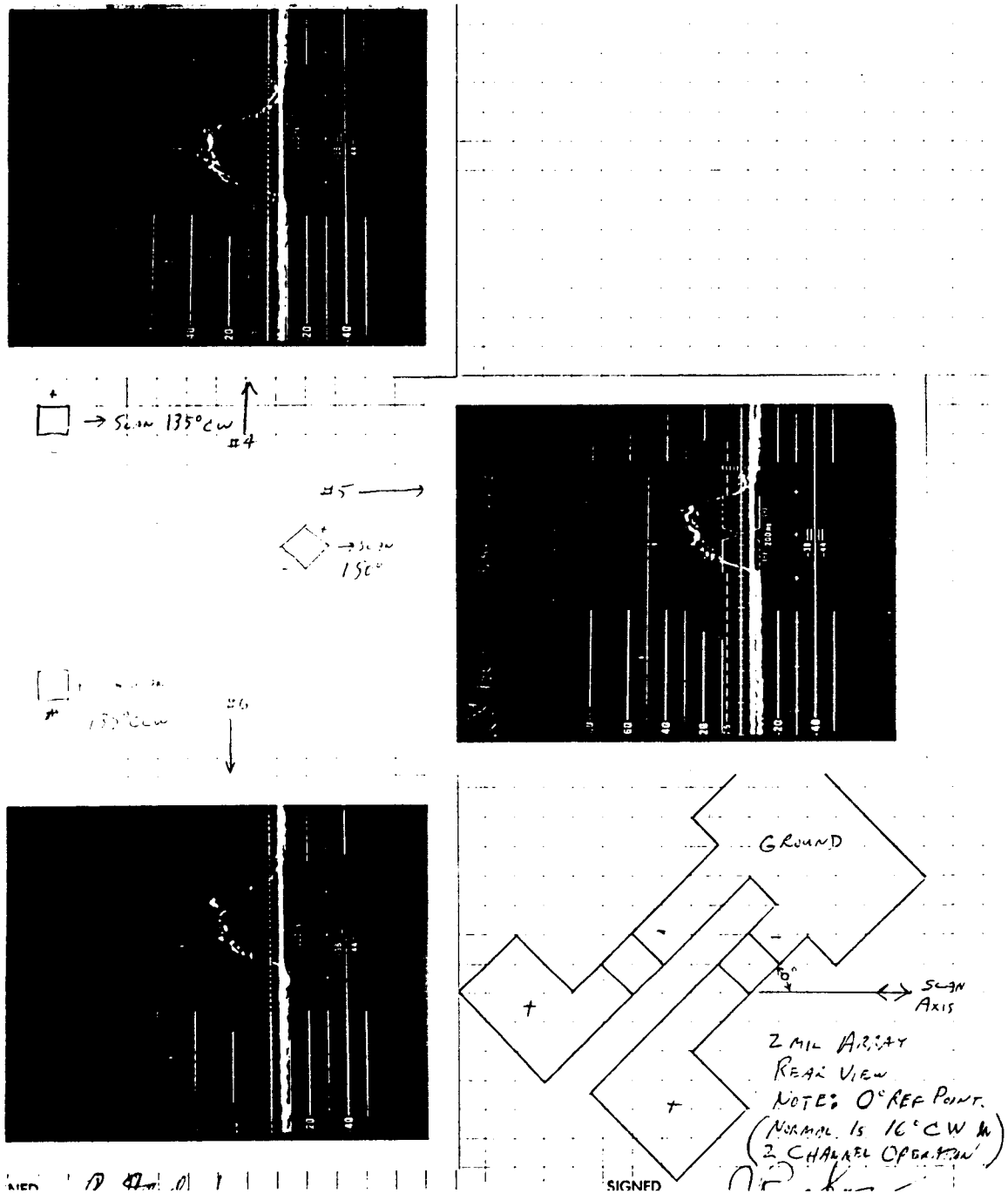

Figure 3.12 Preliminary Experimental Data

4. Summary and Suggestions for Further Work

4.1 Summary and Conclusions

The response of a photoconductive HgCdTe infrared detector to uniform illumination has been studied. It was found that the amount of incident radiation, load resistance, and detector thickness play an important role in the response of the detector.

The response of the detector is taken across a capacitor to remove the DC component of the signal. When the load resistance is much larger or smaller than the detector resistance the AC signal does not change as significantly as when the load resistance is matched to the detector resistance. Therefore, to obtain the maximum change in the AC signal the load resistance should be equal to the detector resistance.

Different levels of illumination cause a significant difference in output voltage with the same fall time. This is important for imagers since different levels of illumination result in various shades of gray on a screen.

The thickness of a detector also plays an important role in the detection of radiation. A relatively thin detector must be used, since increasing the thickness of the detector requires that a larger bias be applied. When the bias is increased the noise increases and a large enough bias can heat the detector. If a row of detectors was fabricated with

varying thickness, different levels of output voltage would be seen for each detector. Therefore, the nonuniform thickness would given erroneous results for a staring array. This would not be as much of a problem in a scanned array since the response of several detector are added together.

Scanned HgCdTe photoconductive infrared detectors have been modeled in five different orientations; scan parallel to the bias, scan opposite to the bias, scan perpendicular to the bias, and two orientations of the scan diagonal to the bias. The results of the modeling are shown in Figures 3.6 - 3.10.

According to the models, the largest response of a scanned detector with the pixel size equal to the detector size occurs when the detector is scanned diagonal to the bias. There is a trade off between the largest response and the fastest fall time. Since the response time when the detector is biased in the same direction as the scan is faster than for a diagonal bias, a higher resolution could be obtained with the scan and bias parallel. Figure 4.1 compares the responses of the five different orientations.

4.2 Suggestions for Further Work

It is possible to add many parameters to this model to generate a more realistic simulation of a scanned infrared detector. The parameters include not only semiconductor influences, but also incident light modifications.

An extended model could add perturbations such as

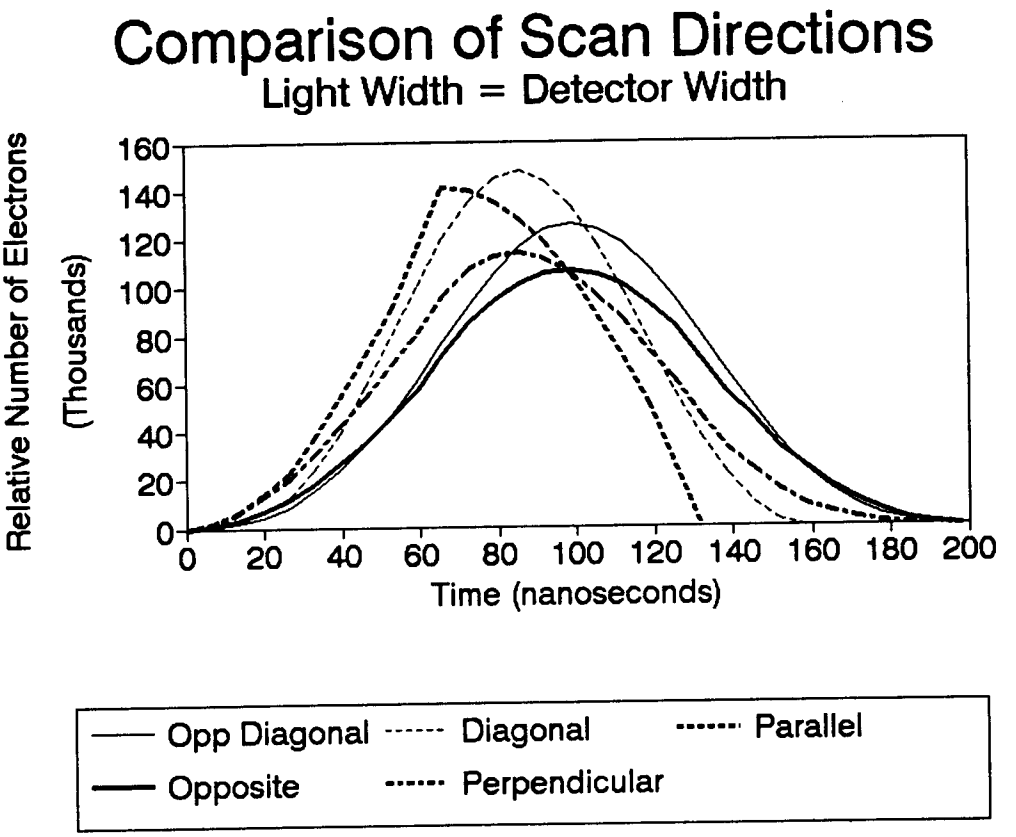

Figure 4.1 Comparison of Scan Directions

recombination, surface state traps, contact resistance, and influences of anti-reflection coatings and passivation on the surface recombination velocity. The effects of biasing and scan speed could also be investigated.

Noise considerations should also be taken into account. These become important at low level illumination, where the number of excited carriers is small. The noise of the detector and the amplified circuit need to be appraised.

A more realistic incident beam would have a Gaussian profile instead of a square edges. The incident beam also contains photons of many different wavelengths (e.g. 4 - 6μm) which were ignored but are in fact absorbed and affect the response.

The circuit model could also be modified. The capacitance and inductance of the detector and packaging could be added to the model. The response of two or more detectors in series or parallel could be investigated.

Verification of the model with experimental data is paramount to the analysis of HgCdTe infrared detectors. Once the experimental data has been compared to the theoretical analysis modifications can be made to the detector and model to yield and improved infrared detector.

References

[1] S. Sze, Physics of Semiconductor Devices, 2nd ed., Wiley-Interscience, New York (1981).

[2] J.I. Pankove, Optical Processes in Semiconductors, Dover, New York (1971).

[3] M. Kinch et al., "Recombination mechanisms in 8-14um HgCdTe," J. Appl. Phys., vol. 44, no. 4, pp. 1649-1663, April 1973.

[4] C. Wolfe, N Holonyak, Jr., and G. Stillman, Physical Properties of Semiconductors, Prentice Hall (1989).

[5] T. Ashley et al., "Optimization of Spatial Resolution in SPRITE detectors," Infrared Physics, vol. 24, no. 1, pp. 25-33, 1984.

[6] Y. Nemirovsky and G. Bahir, "Passivation of mercury cadmium telluride surfaces," J. Vac. Sci. Technol. A, vol. 7, no. 2, pp. 450-459, Mar/Apr 1989.

[7] E. Janik and R. Triboulet, "Ohmic contacts to p-type cadmium telluride and cadmium mercury telluride," J. Phys. D: Appl. Phys., vol. 16, pp. 2333-2340, 1983.

[8] G.D. Davis and W.A. Beck, "Deposition of the reactive metals Al and In onto sputtered and cleaved HgCdTe surfaces," J. Appl. Phys., vol. 60, no. 9, pp. 3150-3156, 1 November 1986.

[9] G.D. Davis and W.A. Beck, "Deposition of the unreactive metal Au onto sputtered and cleaved HgCdTe surfaces," J. Appl. Phys., vol. 60, no. 9, pp. 3157-3161, 1 November 1986.

[10] J. Vincent, Fundamentals of Infrared Detector Operation and Testing, Wiley-Interscience, New York (1990).

[11] I. Spiro and M. Schlessinger, Infrared Technology Fundamentals, Marcel Dekker, New York (1989).

[12] N. Joshi, Photoconductivity Art, Science, and Technology, Marcel Dekker, New York (1990).

[13] A. Rose, Concepts in Photoconductivity and Allied Problems, Wiley-Interscience, New York (1963).

[14] R. Kingston, Detection of Optical and Infrared Radiation, Springer-Verlag, Berlin (1978).

[15] P. Dennis, Photodetectors, Plenum Press, New York (1986).

[16] M. Raine and R. Broudy, "A review of HgCdTe infrared detector technology," SPIE, vol. 124 Modern Utilization of infrared technology III, pp. 80-90, 1977.

[17] C. Snowden, Introduction to Semiconductor Device Modelling, World Scientific, Singapore (1986).

[18] M. Kurata, Numerical Analysis for Semiconductor Devices, Lexington Books, Lexington, MA (1982).

[19] S. Selberherr, Analysis and Simulation of Semiconductor Devices, Springer-Verlag, New York (1984).

[20] E. Rittner, "Electron Processes in Photoconductors," Photoconductivity Conference, pp. 215-129, Nov. 4-6 1954.

[21] A. Kolodny and I. Kidron, "Two-Dimensional effects in intrinsic photoconductive infrared detectors," Infrared Physics, vol. 22, pp. 9-22, 1982.

[22] J. Shappir and A. Kolodny, "The response of small photovoltaic detectors to uniform radiation," IEEE Trans. on Electron Devices, vol. ED-24, no. 8, pp. 1093-1098, August 1977.

[23] F. Szmulowicz et al., "Effect of light on the responsivity and detectivity of traverse and longitudinal detectors," J. Appl. Phys., vol. 60, no. 12, pp. 4300-4307, 15 Dec. 1986.

[24] D. Levy and S. Schacham, "Three-dimensional excess carrier distribution in semiconductor imaging arrays," J. Appl. Phys., vol 64, no. 10, pp. 5230-5233, 15 Nov. 1988.

[25] D. Levy et al., "Three-dimensional analytical simulation of self- and cross-responsivities of photovoltaic detector arrays," IEEE Trans. on Electron Devices, vol. ED-34, no. 10, pp. 2059-2069, October 1987.

[26] K. Misiakos and R. Lindholm, "Exact solution of three-dimensional transport problems using one-dimensional models," J. Appl. Phys., vol. 59, no. 12, pp. 4091-4096, 15 June 1986.

[27] V. Arkhipov et al., "Transient photocurrent due to step-function excitation in disordered materials - computer simulation and analytical treatment," J. Phys. D: Applied Physics, vol. 17, pp. 1469-1475, 1984.

[28] W. Platte, "Photoexcited semiconductor transmission lines," IEE Proc., vol. 136, pt. J, no. 2, pp. 108-110, April 1989.

[29] C. Moglestue, "A Monte Carlo particle study of a semiconductor responding to a light pulse," International Conference on Simulation of Semiconductor Devices and Processes, Univ. Coll. Swansea, Swanswea, Wales, pp. 153-163, 9-12 July 1984.

[30] H. Holloway, "Random-walk treatment of carrier diffusion with surface recombination," J. Appl. Phys., vol. 62, no. 8, pp. 3241-3243, 15 Oct. 1987.

[31] F. Szmulowicz et al., "Photoconductive gain of a longitudinal detector with an arbitrary absorption profile," J. Appl. Phys., vol. 62, no. 1, pp. 310-311, 1 July 1987.

[32] Y. Schacham-Diamand and I. Kidron, "Contact and bulk effects in intrinsic photoconductive infrared detectors," Infrared Physics, vol. 21, pp. 105-115, 1981.

[33] J. Omaggio, "Analysis of dark current in IR detectors on thinned p-type HgCdTe," IEEE Trans. on Electron Devices, vol. 37, no. 1, pp. 141-152, January 1990.

[34] R. Darling, "Surface sensitivity and bias dependence of narrow-gap metal-semiconductor-metal photodetectors," J. Appl. Phys., vol. 60, no. 9, pp. 3157-3161, 15 March 1990.

[35] J. Baars and F. Sorger, "Reststrahlen spectra of HgTe and CdHgTe," Solid State Communications, vol. 10, pp. 875-878, 1972.

[36] E. Finkman and Y. Nemirovsky, "Infrared optical absorption of $Hg_{1-x}Cd_xTe$," J. Appl. Phys., vol. 50, no. 6, pp. 4356-61, June 1979.

[37] J. Brice and P. Capper, Properties of mercury cadmium telluride, INSPEC, New York (1987).

[38] G.L Hansen, J.L. Schmit, and T.N. Casselman, "Energy gap versus alloy composition and temperature in $Hg_{1-x}Cd_xTe$," J. Appl. Phys., vol. 53, no. 10, pp. 7099-7101, October 1982.

[39] G.L. Hanson and J.L. Schmit, "Calculation of intrinsic carrier concentration of $Hg_{1-x}Cd_xTe$," J. Appl. Phys., vol. 54, no. 3, pp.1639-40, March 1983.

[40] P. Knowles and E.E. Schneider, "Cyclotron Resonance in $Hg_{1-x}Cd_xTe$ at 377 Micrometre in the range 77 K - 150 K," Physics Letters, vol. 65A, no. 2, pp. 166-168, 20 February 1978.

[41] M.H. Weiler, Semiconductors and Semimetals, Vol. 16, Academic Press, New York (1981).

[42] E. Finkman, "Determination of band-gap parameters of $Hg_{1-x}Cd_xTe$ based on high-temperature carrier concentration," J. Appl. Phys., vol. 54, no. 4, pp. 1883-6, April 1983.

[43] W. Scott, "Electron Mobility in $Hg_{1-x}Cd_xTe$," J. Appl. Phys., vol. 43, no. 3, pp. 1055-62, March 1972.

[44] Y. Shacham-Diamand and I. Kidron, "Haynes-Shockley experiment on n-type HgCdTe," J. Appl. Phys., vol. 56, no. 4, pp. 1104-8, 15 August 1984.

[45] D.E. Lacklison and G. Duggan, "Determination of the minority carrier mobility of n-type cadmium-mercury-telluride using the Haynes-Shockley method," J. Appl. Phys., vol. 55, no. 12, pp. 4257-65, 15 June 1984.

[46] M.A. Kinch, M.J. Brau, and A. Simmons, "Recombination mechanisms in 8-14μ HgCdTe," J. Appl. Phys., vol. 44, no. 4, pp. 1649-63, April 1973.

[47] R.G. Pratt, J. Hewett, and P. Capper, "Minority-carrier lifetime in doped and undoped n-type $Cd_xHg_{1-x}Te$," J. Appl. Phys., vol. 60, no. 7, pp. 2377-85, October 1986.

[48] M. Czerny and A. Walther, Tables of the Fractional Functions for the Planck Radiation Law, Springer-Verlag, Berlin (1961).

[49] M. Pivovonsky and M. Nagel, Tables of Blackbody Radiation Functions, The MacMillan Company, New York (1961).

[50] Private communication with FLIR Systems Inc.

[51] R. Hall, "Recombination Processes in Semiconductors," The Institution of Electrical Engineers, pp. 923-931, March 1960.

APPENDIX

APPENDIX

List of Symbols

A - area

B - recombination probability

BW - bandwidth

c - speed of light

d - material thickness

D - detectivity

D^* - specific detectivity

D_o - effective diffusion constant

D_e - electron diffusion constant

D_h - hole diffusion constant

$D(\lambda,T)$ - relative cumulative spectral radiance

E - electric field

E_c - conduction band energy

E_g - bandgap energy

E_v - valence band energy

f - volume excitation rate

FTIR - Fourier Transform Infrared

$G(\mathbf{r},t)$ - generation rate

h - Planck's constant

I - incident light intensity

I_d - dark current

J - total current density

J_n - electron current density

J_p - hole current density

k_B - Boltzmann's constant

k - extinction coefficient

L - detector length

L_o - effective diffusion length

L_{Diff} - diffusion length

m_e - electron effective mass

m_{lh} - light hole effective mass

m_{hh} - heavy hole effective mass

n - index of refraction

n(i) - intrinsic carrier concentration

n_o - equilibrium electron concentration

N_c - effective conduction band density of states

N_v - effective valence band density of states

NEP - noise equivalent power

p_o - equilibrium hole concentration

q - electron charge

Q_i - number of incident photons/cm^2

r - position vector

R - reflectivity

$R(\lambda)$ - responsivity

S/N - signal to noise ratio

t - time

x - mole fraction

α - absorption coefficient

Δf - noise bandwidth

$\Delta N(T)$ - partial spectral radiance

Δn - excess electron concentration

Δp - excess hole concentration

Δp_p - initial excess hole concentration

ϵ - dielectric constant

η - quantum efficiency

Γ - gain

λ - wavelength

λ_c - cutoff wavelength

μ_e - electron mobility

μ_h - hole mobility

ρ - charge density

σ - conductivity

$\tau_{n,p}$ - electron and hole lifetimes

τ_{res} - response time

$\tau_{r,f}$ - rise and fall times

ϕ_b - built-in potential of a p-n junction

ϕ_i - intrinsic Fermi level